

**Euler-Lagrange analysis towards representative down-scaling of a 22 m<sup>3</sup> aerobic *S. cerevisiae* fermentation**

Haringa, Cees; Deshmukh, Amit T.; Mudde, Rob; Noorman, Henk

**DOI**

[10.1016/j.ces.2017.01.014](https://doi.org/10.1016/j.ces.2017.01.014)

**Publication date**

2017

**Document Version**

Final published version

**Published in**

Chemical Engineering Science

**Citation (APA)**

Haringa, C., Deshmukh, A. T., Mudde, R., & Noorman, H. (2017). Euler-Lagrange analysis towards representative down-scaling of a 22 m<sup>3</sup> aerobic *S. cerevisiae* fermentation. *Chemical Engineering Science*, 170, 653-669. <https://doi.org/10.1016/j.ces.2017.01.014>

**Important note**

To cite this publication, please use the final published version (if applicable). Please check the document version above.

**Copyright**

Other than for strictly personal use, it is not permitted to download, forward or distribute the text or part of it, without the consent of the author(s) and/or copyright holder(s), unless the work is under an open content license such as Creative Commons.

**Takedown policy**

Please contact us and provide details if you believe this document breaches copyrights. We will remove access to the work immediately and investigate your claim.



# Euler-Lagrange analysis towards representative down-scaling of a 22 m<sup>3</sup> aerobic *S. cerevisiae* fermentation



Cees Haringa<sup>a</sup>, Amit T. Deshmukh<sup>b</sup>, Robert F. Mudde<sup>a</sup>, Henk J. Noorman<sup>b,c,\*</sup>

<sup>a</sup>Transport Phenomena, Chemical Engineering Department, Delft University of Technology, Netherlands

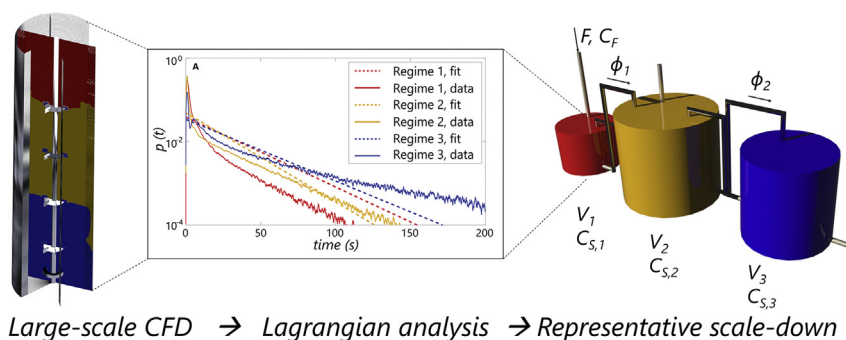
<sup>b</sup>DSM Biotechnology Center, Delft, Netherlands

<sup>c</sup>Bio Separation Technology, Department of Biotechnology, Delft University of Technology, Netherlands

## HIGHLIGHTS

- We propose the scale-down simulator designs based directly on CFD data.
- We present a validated CFD study of a multiphase, large scale fermentor.
- Substrate concentration variations are monitored from the microbial point of view.
- Substrate gradients between fermentors with different relevant timescales are compared.
- Several hitherto used scale-down simulators are compared with the large scale simulation.

## GRAPHICAL ABSTRACT



## ARTICLE INFO

### Article history:

Received 11 August 2016

Received in revised form 22 November 2016

Accepted 9 January 2017

Available online 23 January 2017

### 2015 MSC:

76T10

92-08

### Keywords:

Industrial scale  
Euler-Lagrange  
CFD  
Scale-down  
Fermentation

## ABSTRACT

With reaction timescales equal to or shorter than the circulation time, the ideal mixing assumption typically does not hold for large scale bioreactors. As a consequence large scale gradients in extra-cellular conditions such as the substrate concentration exist, which may significantly impact the metabolism of micro-organisms and thereby the process performance. The influence of extra-cellular variations on the organism can be tested using so-called scale-down simulators, laboratory scale setups where deliberate, controlled fluctuations are imposed in the extra-cellular environment.

The major challenge associated with this scale-down philosophy is to design a scale-down simulator that resembles the extra-cellular environment of the industrial process. Previously, Euler-Lagrange CFD was explored to investigate the large scale environment from the microbial point of view (Haringa et al., 2016a), collecting statistics of the frequency and magnitude of environmental fluctuations that can serve as a basis for scale-down design. In this work, we apply this methodology to a validated CFD simulation of a 22 m<sup>3</sup> aerated fermentation of *S. cerevisiae*, and devise possible scale-down strategies based on this CFD data, both with fluctuating feed profiles and multiple compartments. All designs are deemed feasible within the limitations of current scale-down equipment.

© 2017 The Author(s). Published by Elsevier Ltd. This is an open access article under the CC BY license (<http://creativecommons.org/licenses/by/4.0/>).

**Abbreviations:** SD, scale-down; DO, dissolved oxygen; RTD, residence time distribution; PFR, plug flow reactor; STR, stirred tank reactor; MRF, multiple reference frames; DRW, dynamic random walk.

\* Corresponding author at: DSM Biotechnology Center, Delft, the Netherlands.

E-mail address: [henk.noorman@dsm.com](mailto:henk.noorman@dsm.com) (H.J. Noorman).

## 1. Introduction

In large-scale bioreactors, the timescales associated with the uptake of substrates such as glucose are often of the same order

## Nomenclature

|             |   |                  |  |
|-------------|---|------------------|--|
| $C_s$       | substrate concentration (in broth) [mol/kg]                                     | $Q_g$            | gas flowrate [m <sup>3</sup> /s]           |
| $c_s$       | substrate concentration (mass based) [mg/kg]                                    | $T$              | tank diameter [m]                          |
| $C_x$       | biomass concentration (in broth) [g/kg]   | $t$              | time (general) [s]                         |
| $C_F$       | feed concentration [mol/L]  | $U_g$            | superficial gas velocity [m/s]             |
| $C$         | off-bottom clearance impeller [m]   | $V$              | tank volume [m <sup>3</sup> ]              |
| $D$         | Impeller diameter [m]   | $\alpha$         | gas fraction [-]                           |
| $d_b$       | sauter mean diameter [mm]   | $\Delta t$       | timestep [s]                               |
| $D$         | diffusion coefficient [m <sup>2</sup> /s]                                       | $\Delta C$       | mutual clearance impellers [m]             |
| $F_s$       | substrate feed rate [mol/s]   | $\mu$            | specific growth rate [1/h]                 |
| $F_i$       | feed flowrate [L/L/s]   | $\Omega_{s,max}$ | max. $q_s/q_{s,max}$ on arc trajectory [-] |
| $g$         | gravitational acceleration [m/s <sup>2</sup> ]                                  | $\phi_i$         | circulation flowrate [L/s]                 |
| $H$         | tank height [m]   | $\rho$           | density [kg/m <sup>3</sup> ]               |
| $k_1 a$     | mass transfer coeff. [1/h]  | $\tau_{rxn}$     | uptake timescale of substrate [-]          |
| $K_s$       | affinity constant for substrate [mol/kg]  | $\tau_{circ}$    | circulation timescale [-]                  |
| $Y_{sx}$    | max. biomass yield on substrate [Cmol <sub>x</sub> /Cmol <sub>s</sub> ]         | $\tau_{95}$      | mixing time [-]                            |
| $M$         | Nm [Impeller moment]  | $\tau_{arc}$     | arc-time [-]                               |
| $m_s$       | maintenance coefficient [mol <sub>s</sub> /Cmol <sub>x</sub> /h]                | $\tau_i$         | mean residence time, vessel $i$ [-]        |
| $N_c$       | total number grid cells [-]   | $\gamma$         | surface tension [N/m]                      |
| $N_p$       | total number particles [-]  | $\bar{y}$        | volume-average of $y$ [-]                  |
| $N_s$       | impeller revolutions [1/s]  | $\bar{\tau}_i$   | mean residence time, regime $i$ [-]        |
| $P$         | power input [W]   | $p(y)$           | probability of $y$ [-]                     |
| $q_p$       | specific production rate of product [mol <sub>p</sub> /Cmol <sub>x</sub> /h]    | $\sigma(y)$      | standard deviation of $y$ [-]              |
| $q_s$       | specific uptake rate of substrate [mol <sub>s</sub> /Cmol <sub>x</sub> /s]      | $Po_g$           | power number (gassed) [-]                  |
| $q_{s,max}$ | max. specific uptake rate of substrate [mol <sub>s</sub> /Cmol <sub>x</sub> /s] | $Sc_T$           | Schmidt number, turbulent [-]              |
| $q_{ref}$   | reference $q_s/q_{s,max}$ [-]   | $St$             | Stokes number [-]                          |
| $QM$        | Maximum $q_s/q_{s,max}$ obtained in SD simulator [-]                            |                  |  |

of magnitude as the vessel circulation time, representative of mixing in the system. As a result, the ideal mixing assumption does not hold for many industrial bioprocesses, and thus large-scale substrate gradients exist in the reactor (Haringa et al., 2016; Enfors et al., 2001; Oosterhuis and Kossen, 1984). From the point of view of micro-organisms inside the vessel, this causes (strong) temporal variations in the extra-cellular substrate concentration  $C_s$ . These variations may have an effect on their metabolism, which continuously needs to adapt to variations in substrate availability. Similar to substrate gradients, gradients in dissolved oxygen (DO), pH, temperature and other process variables may be found.

Since large-scale gradients can have a critical influence on the overall process performance, they should be accounted for during process development. To this end scale-down simulators (SD-simulators) have been developed; laboratory scale systems in which micro-organisms are subjected to temporal variations in a given process parameter (Neubauer and Junne, 2010; Wang et al., 2015). These may be well defined variations (e.g. de Jonge et al., 2011; Sweere et al., 1988a; Ying Lin and Neubauer, 2000), typically imposed by a fluctuating feed in a single vessel, in order to study the direct impact of variations on the metabolism. Alternatively, fluctuations with a distributed duration can be imposed, being more representative of an actual industrial situation (e.g. Sweere et al., 1988b; Heins et al., 2015; Limberg et al., 2016; Lemoine et al., 2015). This is often done by placing multiple reactors, operating under different conditions, in a flow loop.

In order to obtain directly applicable insight about the effect of environmental variations in industrial scale reactors, the duration and magnitude of environmental variations imposed in SD-simulators should reflect the variations encountered at the large scale. Statistics of the distribution of the parameters involved are, however, rarely available for industrial scale reactors. To approximate the industrial environment, current SD-simulators are often set to achieve a fluctuation duration in the order of the industrial 95% mixing time ( $\tau_{95}$ ), typically between 60 and 600 s. In previous

work, we employed Computational Fluid Dynamics (CFD) simulations to show that this is too long; global concentration variations occurred on average in the order of the circulation time  $\tau_{circ}$ , with local variations occurring at shorter timescales (Haringa et al., 2016). While the currently generation of SD-simulators certainly has its merits for metabolic model development, industrial conditions are often poorly represented.

CFD can be exploited to obtain more detailed insight in the fermentation environment, without the limitations of experimental investigation (Wang et al., 2015; Delvigne et al., 2006; Lapin et al., 2004, 2006; Delafosse et al., 2015; Pigou and Morchain, 2015). In particular, the Euler-Lagrange approach developed by Lapin et al. (2004, 2006) is highly valuable, as it allows one to study the environment from the microbial point of view by registering *condition vs. time* series, referred to as (micro-organism) lifelines. These series can be analyzed to generate statistics on the duration and magnitude of, for example, substrate concentration variations (Haringa et al., 2016; McClure et al., 2016) providing environmental fluctuation statistics that can serve as a basis of design for representative SD-simulators.

Previously, we presented a methodology to analyze lifelines obtained with Euler-Lagrange CFD in order to acquire such fluctuation statistics, showcasing our approach on a simplified industrial *P. chrysogenum* fermentation. Here we apply our approach to a more representative case, supported by well documented experimental data: the aerated *S. cerevisiae* fermentation conducted in a 22 m<sup>3</sup> fermentor in Stavanger (Enfors et al., 2001; Larsson et al., 1996; Vrabel et al., 1999, 2000, 2001). In this paper we (1) validate the simulation of a large scale fermentor, (2) show how micro-organisms experience the large scale substrate concentration gradient, (3) compare the results between two case studies, showing how the ratio between relevant timescales influences the environment that microbes experience and (4) propose simple designs for SD-simulators (both containing multiple compartments and varying feed strategies), that reasonably replicate industrial

conditions. With this, we show, for the first time, scale-down simulator design proposals that are directly based on CFD simulations of an industrial scale fermentor.

## 2. Materials and methods

We monitor the extra-cellular substrate concentration  $C_s$  in a glucose-limited 22 m<sup>3</sup> fermentor. The dissolved oxygen concentration was not monitored; in the experiment of Larsson et al., the dissolved oxygen concentration  $DO$  was above 30% and no oxygen limitations are expected (Larsson et al., 1996). Lagrangian particle tracking is used to register variations in  $C_s$  from the microbial point of view.

**Geometry and operating conditions** The simulated fermentor had a diameter  $T = 2.09$  m and a liquid filled height  $H = 6.55$  m, containing 4 Rushton impellers ( $D = 0.7$  m). The off-bottom impeller clearance  $C = 1.12$  m, the impeller spacing  $\Delta C = 1.46$  m. A graphical overview of the reactor is given in Fig. 1(A). The agitation rate was set to  $N = 2.22$  1/s. Gas was fed via a ring sparger located at  $H_s = 0.47$  m with a gas flow rate  $Q_g = 0.182$  N m<sup>3</sup>/s, resulting in a gas-flow number  $Q_g/ND^3 = 0.24$  and Froude number  $N^2D/g = 0.35$ . Under these conditions the bottom impeller is expected to be in the loading regime (Lee and Dudukovic, 2014), while the other impellers operate under dispersion conditions. The rheology of the broth was assumed to be equal to water ( $\rho = 1000$  kg/m<sup>3</sup>,  $\mu = 0.001$  Pa s), the air-water surface tension  $\gamma = 0.072$  N/m.

**Simulation setup.** Simulations were conducted in ANSYS FLUENT 15.7 with the standard  $k - \epsilon$  turbulence model and the multiple reference frame (MRF) model to simulate the impeller motion. The Euler-Euler approach was used for gas-liquid modeling. Gunyol and Mudde (2009) showed that assuming a single bubble size in the range of 3–5 mm (based on Barigou and Greaves, 1992; Laakkonen et al., 2005a,b) resulted in poor predictions of the gas hold-up  $\alpha$ , while a population balance approach gave good results. We therefore used the discrete population balance model,

with 16 diameter classes ranging between 0.5 and 16 mm, with a ratio-exponent of 1. While Gunyol et al. used only 6 bubble classes, the simulated flow- and gas holdup fields are highly similar to their work, with a slightly higher Sauter mean diameter being reported (9.5–10 mm versus 8.9 mm in the current work). Consequently, no strong effect of the number of size classes is expected on the results. The break-up and coalescence kernels of Luo and Svendsen (1996) were employed. Bubble drag was modeled using Fluent's Universal drag model, based on the drag model of Ishii and Zuber (1979). Dispersed phase turbulence was included using the mixture model with shares  $k$  and  $\epsilon$  equations between the phases.

Based on the results of Gunyol et al., a 60° domain was modeled (Fig. 1(B)), with periodic boundary conditions on the sides. This periodicity splits the feed over 6 angular positions; due to the strong axial nature of the substrate gradient, this assumption does not strongly affect the overall glucose distribution. The presence of 6 rather than 4 baffles was found to have little influence on the overall flow (Gunyol and Mudde, 2009). All walls were no-slip boundaries for liquid and free-slip for gas, only at the impellers a no-slip condition was applied for both phases to account for the accumulation of gas in the trailing vortices behind the blade. A total tank height of  $H_T = 11$  m was modeled to allow for expansion of the fluid due to gassing, using a gas-backflow pressure outlet as top boundary condition. A structured hexahedral mesh containing 611,000 grid cells was used, shown in Fig. 1(B). During particle tracking, the headspace was removed and a degassing condition was imposed at the top to prevent particles from getting stuck in the headspace. Further details on the solution procedure can be found in Appendix A.

**Fermentation details.** A fixed biomass concentration  $C_x = 10$  g/L was used, with a constant glucose feed rate  $F = 52$  kg/h (as a 50 wt% solution) and constant liquid-filled height. As reported experimentally in Larsson et al. (1996),  $C_x$  increases in time; in this simulation  $C_x$  is fixed to yield a temporal snapshot, focusing on second-minute scale fluctuations and assuming slow processes such as growth to be quasi-steady. The fermentation was conducted with the *S. cerevisiae* strain CBS8066 (Larsson et al., 1996). Postma et al. (1989a,b) studied CBS8066 in steady-state chemostat fermentors and noted that the relation between the residual glucose concentration and dilution rate did not follow classical Monod kinetics. Suarez-Mendez et al. did report a good agreement with Monod kinetics under oscillating feed conditions (400 s feed cycles, different strain) (Suarez-Mendez et al., 2014). Combined, these studies hint availability of glucose transporters adapts to the growth rate  $\mu$  (Heijnen and Romein, 1995). When exposed to rapid extra-cellular variations, the slow dynamics of transporter synthesis and degradation result in a pseud-steady maximum transport capacity, and Monod behavior is retrieved. Hence, we did assume Monod kinetics hold under the simulated conditions, since the overall extra-cellular conditions are in steady state, and the fluctuations registered by micro-organisms are rapid. Hence,  $q_s = q_{s,max} \cdot C_s / (K_s + C_s)$  mol/g<sub>dw</sub>/h, with  $C_s$  the local glucose concentration in mol/kg. We adopted the kinetic parameters used by Larsson et al. (1996):  $q_{s,max} = 0.00944$  mol/g/h and  $K_s = 0.001$  mol/kg.

**Particle tracking and reaction coupling.** Lapin et al. (2004, 2006) employed complex reaction models, coupled to the individual particles in their work. Since we apply simple Monod kinetics,  $q_s$  instantaneously adapts to the local  $C_s$  and the reaction kinetics can be coupled to the liquid phase rather than particle phase (Haringa et al., 2016). Combined with the steady-state MRF impeller modeling approach, this results in a steady state flow field, as well as steady-state  $C_s$  and  $q_s$ -fields with a fixed gradient in space. These fields do not require updating during the particle tracking phase and are hence frozen after flow convergence (Haringa et al., 2016).

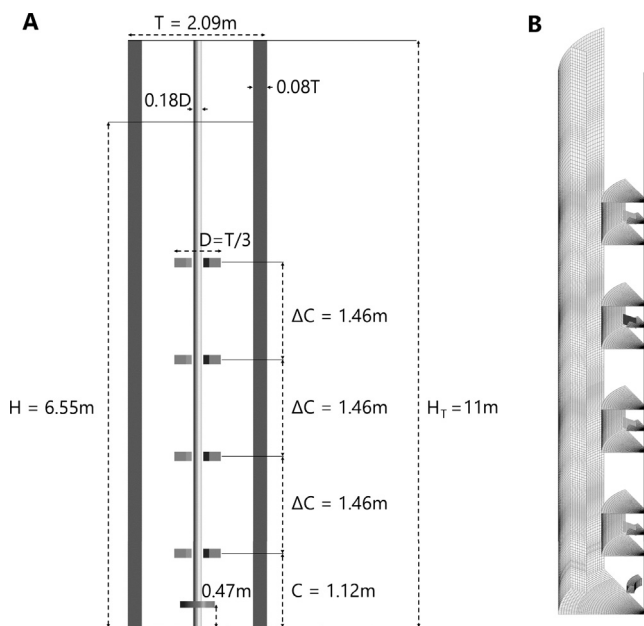


**Fig. 1.** (A) Graphical overview of the simulated domain with all relevant sizes. Part of the headspace is removed when the degassing boundary condition is used. (B) Meshed section of the reactor (after headspace removal). Local refinement is applied in the impeller discharge stream, and regions where flow-loops are expected to meet. The MRF-boundaries are displayed around each impeller.

With the reaction coupled to the liquid phase, particles only register the local extra-cellular  $C_s$ , but do not influence the flow- or  $C_s$  fields. This means there is no lower limit on  $N_p$  to achieve properly resolved gradients (Haringa et al., 2017). Here,  $N_p$  is chosen such that reasonably converged fluctuation statistics are obtained without requiring excessive simulation times. A total of  $N_p = 12,500$  particles were added after flow convergence, they were tracked for 1190 s. With an organism size of 5–10  $\mu\text{m}$ , the particle Stokes number  $St \ll 1$  and particles are treated as massless tracers. Turbulent motions were superimposed via the discrete random walk (DRW) model. For each particle, the instantaneously observed  $C_s$  is recorded with a time resolution of 0.03 s via a user defined function; this time-series is referred to as the organism lifeline.

#### Validation parameters

For validation purposes, the overall gas holdup  $\bar{\alpha}$ , gassed impeller power numbers  $Po_g$ , overall  $k_L a$ , mixing time  $\tau_{95}$  and the global mean bubble diameter  $\bar{d}_b$  were studied. The gas holdup was determined by volume-averaging the local gas holdup  $\alpha$  according to Eq. (1):

$$\bar{\alpha} = \frac{\sum V_c \alpha_c}{\sum V_c} \quad (1)$$

using the cell volume  $V_c$  as a weight. Similarly, the global mean bubble diameter was determined by volume-averaging the local Sauter mean diameter, weighted by the gas volume rather than the total cell volume (Eq. (2)):

$$\bar{d}_b = \frac{\sum V_c \alpha_c d_{b,c}}{\sum V_c \alpha_c} \quad (2)$$

The power number was calculated from the torque exerted on the individual impellers (Eq. (3)):

$$Po = 6 \cdot \frac{2\pi M}{\rho N^2 D^5} \quad (3)$$

with  $M$  the rotational moment. The factor 6 is included due to the periodic domain. To calculate the inter-phase mass transfer coefficient  $k_L$ , we used the eddy cell model of Lamont and Scott (1970), Eq. (4), which was shown by Gimbut et al. (2009) to yield good results.

$$k_L = 0.4 \cdot D_i^{0.5} \frac{\epsilon^{0.25}}{\nu_i} \quad (4)$$

Following Gimbut et al., the interfacial area of the bubbles  $a$  was calculated taking into account bubble deformation via Eq. (5), which estimates the ratio between the major and minor ellipsoid axes of a deformed bubble:

$$R = 1 + 0.163(Eo)^{0.757} \quad (5)$$

With  $Eo = g\Delta\rho d_b/\gamma$  being the Eötvös number. Using the local Sauter mean diameter  $d_b$  to determine the bubble volume, the ellipsoidal bubble's surface area can be calculated straightforwardly. The overall  $k_L a$  is calculated by volume averaging, similar to  $\alpha$ . The Eulerian mixing time  $\tau_{95}$  was determined by placing a virtual probes at heights  $Y = 1.12, 4.04, 6.56$  m, equal to the experiment, and determining when  $0.95 < C_s/\bar{C}_s < 1.05$ . A Lagrangian mixing experiment was conducted with 5,750,000 particles, registering when  $0.95 < C_p/\bar{C}_p < 1.05$  with  $C_p$  the particle concentration. A 4 s moving-average filter was used for noise removal, the filter time was determined via a sensitivity study. More information on the mixing study is provided in Appendix A.

## 2.1. Data analysis

A brief summary of our data analysis approach is presented here, for a full description we refer to (Haringa et al., 2016). All analysis work was done in MATLAB R2015b (v8.6.0).

### 2.1.1. Metabolic regimes

Since we are concerned with how micro-organism experience extra-cellular variations, the recorded organism lifelines are expressed in terms of the normalized biomass specific glucose uptake rate,  $q_s/q_{s,max}$  versus time  $t$ , rather than  $C_s$  versus  $t$ . Our analysis aims to translate the fluctuations observed along a large collection of lifelines to a small set of duration and magnitude distributions that can serve as a basis for SD-simulator design. The first consideration is: fluctuations with respect to which reference value?

As micro-organisms have no notion of their position in space, we do not use a spatial reference point to determine (circulation) time distributions (Choi et al., 2004; Delafosse et al., 2015). Rather, reference points within  $q_s$ -space are chosen. This  $q_s$ -space is divided in (metabolic) regimes, the boundaries of which are typically based on metabolic responses (starvation/saturation conditions, overflow regimes, and so on). Alternatively, regimes can be based on dominant values in the volumetric  $q_s$ -distribution. A proper choice of regimes may simplify the analysis; for example, the saturated uptake in a glucose-excess regime makes the magnitude of  $q_s$ -variations in this regime irrelevant.

Prior to the analysis, the trajectories are smoothed and filtered to remove rapid turbulent fluctuations that would skew fluctuation statistics towards short timescales (Haringa et al., 2016). These rapid variations have a low magnitude, and likely have little effect on the organism (Linkès et al., 2014). Smoothing is performed using a moving-average filter, with a filter window equal to the Lagrangian timescale  $\tau_L = 0.15k/\epsilon$  that is representative for turbulent motions imposed by the DRW model. A dispersed rather than sharp regime boundary is applied to remove rapid consecutive regime-crossings. In addition, extreme jumps in  $q_s$  may be registered if a particle moves close to a gas-filled trailing vortex, due to the finite accuracy of the numerical particle trajectory integration. Such outliers are filtered out by a rate-of-change filter. Additional information on filter implementations can be found in Appendix B.

### 2.1.2. Transitions and residence times

The regime residence time quantifies the time spent inside a given regime by a particle during a single visit, yielding a residence time distributions (RTD) when analyzing many visits. A regime transition is recorded when the  $q_s/q_{s,max}$ -lifeline of an organism crosses the  $q_s/q_{s,max}$ -value associated with a regime boundary. The regime of origin and destination is registered for each transition, providing insight in how organisms move through the reactor.

When fluctuations *within* a regime are relevant, c.q. when local variations in  $C_s$  significantly impact the magnitude of  $q_s$ , an additional 'arc analysis' can be conducted (Haringa et al., 2016). This requires an additional reference value for  $q_{ref}$  within the bounds of the relevant regime, for example the mean regime  $q_s/q_{s,max}$ . The 'arc' refers to the section of the lifeline in between two crossings of  $q_{ref}$ , with the arc-time ( $\tau_{arc}$ ) describing the time between two consecutive crossings of the reference value. For many events, this yields an intra-regime circulation time distribution. The arc magnitude is quantified by registering the extreme in  $q_s/q_{s,max}$  (the minimum if the particle moves down from  $q_{ref}$  and maximum if it moves up), and is named  $\Omega_{s,max}$ .

To summarize, our proposed methodology reads:

- Determine regimes based on the metabolic response, or dominant conditions in the reactor.
- Determine how particles move between regimes from the micro-organism lifelines.
- Determine the residence time distribution for each regime, as well as follow-up behavior.
- (optional) Quantify oscillations *within* relevant regimes compared to an intra-regime reference value.

### 3. Results and discussion

#### 3.1. Validation

Experimental and simulated values for the studied validation parameters are listed in Table 1. The simulated power number and gas holdup  $\alpha$  are in good agreement with experimental data. The volume-averaged  $k_L a$  is somewhat underestimated, which could be due to an overestimation of the bubble size; at  $\bar{d}_b = 8.9$  mm the mean size is high compared to lab/pilot-scale studies (Barigou and Greaves, 1992; Laakkonen et al., 2005a,b). Unfortunately, this observation cannot be verified, lacking experimental data on  $d_b$  for the current fermentation. Still, the agreement in  $k_L a$  is very decent considering that broth is a complex, surfactant-laden substance. Over-prediction of the number fraction in the large bubble size classes is a known problem for the Luo kernel (Wang et al., 2005). As  $\alpha$  is properly predicted, and  $d_b$  does not directly impact our work, we did not attempt the use of other kernels. The volumetric gas distribution, Fig. 2(A), shows that the expected loading flow regime is indeed retrieved for the bottom impeller.

##### 3.1.1. Mixing behavior

Experimentally, two different values for  $\tau_{95}$  are available from different studies (Noorman, 2011; Vrabel et al., 1999), both are reported in Table 1. From the Lagrangian mixing data  $\tau_{95} = 183$  s, a 10–25% overestimation compared to the experimental data, which is acceptable considering the complexity of the simulation and typical experimental variation in mixing studies. The tracer mass balance was not fully closed in Eulerian mixing simulations, leading to small temporal variations in the total tracer amount, an issue noted earlier for multiphase MRF simulations (Gunyol et al., 2009). This was least pronounced when using the pressure outlet boundary condition, (which gave  $\tau_{95} \approx 169$  s), but due to the full conservation of particle number, the Lagrangian result is deemed the most reliable. A full discussion of all mixing data is added in Appendix A.

The tracer response dynamics deviate from the experimental curve reported by Noorman (2011), both for the Eulerian and Lagrangian approach, as shown in Fig. 3. A feasible explanation is a difference in the dominant transport mechanism (Lubbert and Larson, 1990; Noorman, 2011). In bubbly flows convective mixing

arising from the bubble motion dominates, whereas in strongly turbulent flows where eddy diffusion is dominant. With the assumptions made in our simulations (mixture turbulence model, no turbulence interaction force), it appears the liquid phase mixing behavior resembles that of a single phase liquid, aside from stronger axial motion caused by the gas flow. A consequence of this axial motion is that tuning the turbulent Schmidt number  $Sc_T$  in the Eulerian mixing experiments did not lead to a consistent improvement in  $\tau_{95}$ . This contrasts the observations made in single-phase, multi-impeller mixing studies (Haringa et al., 2016; Gunyol et al., 2009; Montante et al., 2005; Delafosse et al., 2014). We believe axial mixing is underestimated in single-phase flow simulations (Bujalski et al., 2002; Jaworski et al., 2000), and this underestimation is reduced due to the improved axial transport resulting from the gas flow. A further discussion on  $\tau_{95}$  and  $Sc_T$  can be found in Appendix A.

##### 3.1.2. Substrate concentration gradient

Fig. 2(B) shows the simulated concentration gradient (degassing boundary condition,  $Sc_T = 0.7$ ). In agreement with previous simulations (Larsson et al., 1996; Gunyol et al., 2009), the weak axial mixing of Rushton turbines leads to strong axial heterogeneity. Despite the upward motion imposed by the gas, the overall flow is impeller-dominated leading to clear compartment formation within the observed gradient. Still, the flow barrier that typically exists in Rushton driven flows is less pronounced than for a single phase simulation, consistent with the somewhat improved axial mixing noted above. The mass-based glucose concentration  $c_s$  is in fair agreement with experimental values (Larsson et al., 1996), considering the inherent approximations made both in the CFD and metabolic models. At the top probe  $c_s$  is over-predicted by a factor 2, but due to the strong local gradient, the value is very sensitive to the exact position: a few cm down,  $c_s = 50 - 60$  mg/L. Aside from the value at the top probe, changing the top boundary condition and  $Sc_T$  had little effect on the concentration gradient; this is further discussed in Appendix B.

The clear compartmentalization of the substrate gradient contrasts the observations made in the *P. chrysogenum* case study reported earlier (Haringa et al., 2016), which contained a much smoother gradient. This difference in behavior arises from the ratio between the circulation time  $\tau_{circ}$  ( $\tau_{circ} \approx \tau_{95}/4$  (Noorman, 2011)) and reaction time  $\tau_{rxn} = C_s/(q_s C_x)$ . Under substrate limited conditions  $\tau_{rxn}$  can be estimated by assuming the limit  $C_s \rightarrow 0$  for Monod kinetics, yielding  $\tau_{rxn} = K_s/(C_x q_{s,max})$ . In the *P. chrysogenum* case,  $\tau_{circ} = 18.2$  s and  $\tau_{rxn, C_s \rightarrow 0} = 0.32$  s, over an order of magnitude difference. As a result, the *P. chrysogenum* case contains a strong substrate gradient manifesting *within* the circulation loop of the top impeller. In the current case study the timescales are of the same order,  $\tau_{circ} = 46.5$  s and  $\tau_{rxn, C_s \rightarrow 0} = 38$  s. While yielding a significant substrate gradient overall, the broth *within* individual circulation loops is well mixed. Roughly estimating the per-loop circulation time as  $\tau_{circ}/N_{loops}$  gives  $46.5/8 = 5.8$  s, showing that intra-loop mixing is rapid compared to reaction, supporting the observed intra-loop homogeneity.

The difference in compartmentalization behavior is clearly visible in the volumetric substrate distribution, Fig. 4. In the *S. cerevisiae* case, several sharp peaks are observed, associated with the individual, well-mixed compartments. In the *P. chrysogenum* case, a large section of the domain is completely devoid of substrate and a small section has sugar in excess, with a gradual change in between.

#### 3.2. Residence time distributions

We have applied the Lagrangian analysis methodology discussed in Section 2.1 to the *S. cerevisiae* simulation. The metabolic regime

**Table 1**

Global validation parameters for the simulation.  $k_L a$  is retrieved from Larsson et al. (1996). Experimental gas holdup is reported for water (Vrabel et al., 1999). Mixing times differ between sources, the lower value is retrieved from Noorman (2011), the higher value was reported by Vrabel et al. (1999). Power numbers are retrieved from previously unpublished data of the Stavanger experiments.

| Parameter   | Simulation | Experimental | Exp. method            |
|-------------|------------|--------------|------------------------|
| $\alpha$    | 17.6       | 17.1         | Height increase        |
| $PO_g$      | 9.6        | 9.2          | Torque                 |
| $k_L a$     | 144 1/h    | 180 1/h      | O <sub>2</sub> balance |
| $\tau_{95}$ | 183 s      | 147–166 s    | Probe (bottom)         |
| $\bar{d}_b$ | 8.9 mm     | n/a          | n/a                    |

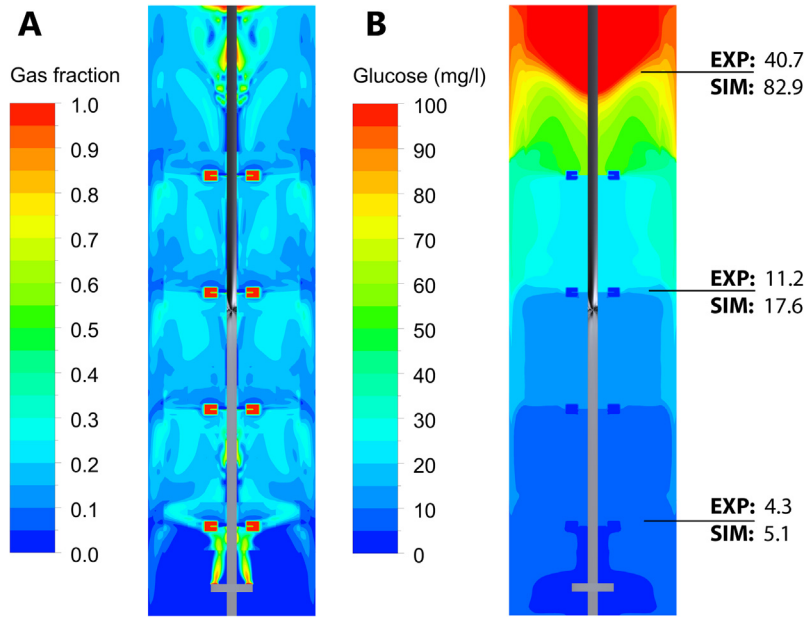


**Fig. 2.** (A) Gas holdup in the vessel. Close to the top there are some artifacts of the degassing method. (B) Glucose concentration profile (top feed). Experimental values (mg/L) are retrieved from Larsson et al. (1996).

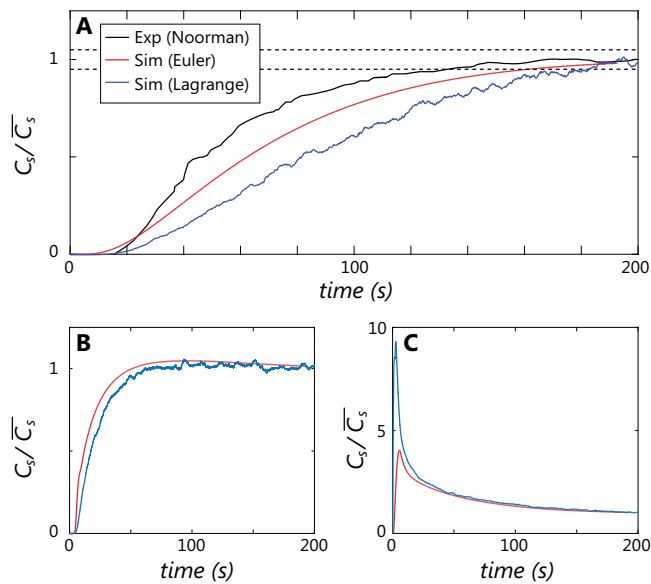


**Fig. 3.** Mixing curves for the  $N = 2.22$  1/s and  $Q_g = 0.182$  m<sup>3</sup>/s. The experimental data was retrieved from Noorman (2011) which yields a lower mixing time than (Vrábel et al., 1999). Red curves show Eulerian tracer data (pressure outlet,  $Sc_T = 0.7$ ), blue curves show Lagrangian particle data (smoothed over a period of 4 s for noise removal, degassing b.c.,  $Sc_T = 0.7$ ) (A) bottom probe. (B) Middle probe. (C) Top probe.

division in an excess, limitation and starvation zone, applied in the *P. chrysogenum* case is not applicable here due to the lack of a substrate excess zone. Instead, we construct an alternative regime division based on the Crabtree-effect, the aerobic production of ethanol resulting from saturation of the pyruvate to acetyl-CoA (either directly or via acetaldehyde) processing pathway (Postma et al., 1989a). Strain CBS8066 has been widely studied (e.g. Postma et al., 1989a,b; Verduyn et al., 1990, 1992; Van Urk et al., 1989; Pham et al., 1998) in this respect, revealing that the onset of the Crabtree effect lies around  $C_s = 0.22$  mmol/L (Postma et al., 1989a), which equals  $q_s/q_{s,max} \approx 0.2$ . We use this value as a basis for the first regime. Ethanol is predicted to be produced in the top

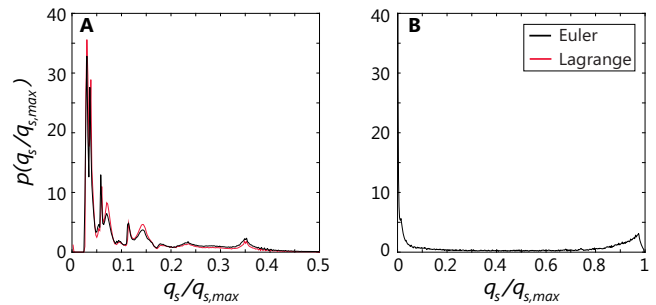


**Fig. 4.** Normalized volumetric distribution function of  $q_s/q_{s,max}$  in the tank domain; the y-axis is scaled such that the area under each curve is 1. (A) Distribution function for the current *S. cerevisiae* simulation, both from the Eulerian and Lagrangian viewpoint. The effect of compartment formation in the current case is clearly visible. The Eulerian distribution results from the steady-state  $q_s$  field; in case an unsteady method is used, the field should be time-averaged. The Lagrangian distribution represents the overall distribution registered by particles, taken over all lifelines and timesteps. (B) The *P. chrysogenum* simulation (right) described in Haringa et al. (2016).

of the vessel, consistent with experimental observations (Noorman, 2011). In the bulk of the vessel, sufficient glucose is available. Near the bottom consumption of ethanol is reported to occur (Noorman, 2011); the exact onset of ethanol consumption is, however, unknown and we cannot base a regime boundary on this phenomenon.

In Fig. 4(A) two closely spaced, sharp peaks are visible for  $q_s/q_{s,max} < 0.05$ , indicating that a large fraction of the liquid volume has a low glucose availability, with a relatively constant  $q_s$ . When designing a laboratory scale representation of this industrial fermentor, this low-uptake regime can be approximated by a single  $q_s/q_{s,max}$  value, making  $q_s/q_{s,max} = 0.05$  a convenient boundary for the lower regime. The above considerations lead to the following regime division:

- Regime 1:  $q_s/q_{s,max} > 0.2$ , Ethanol production.
- Regime 2:  $0.05 < q_s/q_{s,max} < 0.2$ , Glucose limitation.
- Regime 3:  $q_s/q_{s,max} < 0.05$ , Low glucose availability (possibly ethanol consumption).

Considering the volumetric distribution of the regimes in the fermentor, the interfaces between regime 1 and 2 and regime 2 and 3 coincide with the first (top) impeller and third impeller, respectively. Due to the steady-state background fields in this work, these interfaces are fixed both in space and time from the Eulerian perspective. This notion facilitates the subsequent analysis, as specific features observed in the Lagrangian residence time distributions (RTDs) can be linked to Eulerian observations directly. For example, the position of these interfaces relative to the circulation loops originating from these impellers has a notable impact on the RTDs, as is discussed later.

Since the regime division is based on the instantaneous  $q_s$  (and  $C_s$ , being directly coupled in case of Monod kinetics), linking Lagrangian observations with Eulerian flow features is much more difficult when the background fields are unsteady. In that case, the spatial regime distribution is continuously changing, and the regime interfaces locations will be dynamic. Of course, the Lagrangian lifeline methodology and the regime-analysis in themselves are compatible with unsteady simulations. Regime transitions and RTDs can be determined, whether the background fields are steady or unsteady.

From the Eulerian perspective, the regimes 1, 2 and 3 cover 23/41/36% of the total liquid volume, respectively. Taking the Lagrangian perspective, the regime division is determined by registering the average time spent by particles inside each regime, yielding 18/42/40%, respectively. This is a notable difference, not observed in earlier single-phase simulations (Haringa et al., 2016). It is difficult to pinpoint the exact reason of this difference, considering the good agreement between the observed regime distributions from the two perspectives (Fig. 4(A)); it may simply be a statistical fluke originating from the slow convergence of the regime statistics.

The RTD for each regime, constructed by recording the duration of individual regime exposures, is reported Fig. 5. A *log-lin* scale is used to highlight certain features of the RTDs: a constant slope on this plot signifies an exponential decay in probability, providing information about the typical circulation behavior. Changes in slope hint at different circulation patterns with their own associated time constants. For each trajectory the mean residence time

is calculated as  $\bar{\tau}_x = \sum(c_{t,x}t_{res,x})/\sum(c_{t,x})$ ,  $c_{t,x}$  being the number of counts for a given residence time  $t_{res}$  in distribution  $x$ . To study the regime follow-up behavior, the following trajectories are discriminated (visually outlined in Fig. 5(C) and (D)):

- a: From regime 1, in 2, back to 1.
- b: From regime 1, in 2, to 3.
- c: From regime 3, in 2, back to 3.
- d: From regime 3, in 2, to 1.
- e: From regime 2, in 1, back to 2.
- f: From regime 2, in 3, back to 2.

Of all trajectories entering regime 2 from 1, only 8.7% are of type *b*, all others being type *a* (in the converse direction, 18.7% are type *d*). As the regime 1–2 interface coincides with the top impeller, by far most registered interface crossings concern particles completing a single circulation in one of the loops originating from the top impeller. This trajectory lasts < 6 s, yielding the RTD peak clearly visible in the inset of Fig. 5(A). Similar single-circulation trajectories are found in distributions *c, e, f*.

Since all regimes enclose multiple circulation loops, multiple slopes are distinguished in each RTD. The mid-range (6–40 s for regime 2, and 6–20/6–30 s for regimes 1 and 3, respectively) is a complex combination of trajectories through several circulation loops, whereas the long term behavior reflects particles residing in a single region for a long time. It is visible that for  $t > 40$  s all type *a–d* trajectories have similar RTDs; these particles have completed several circulations within the regime 2 region, and their behavior is no longer influenced by their regime of origin or destination. As trajectories *b* and *d* have to fully cross the regime 2 region a lag-time of 6 s is registered (Fig. 5(A), inset). The symmetry of the *b* and *d* RTD is noteworthy, consistent with the notion that the flow is still dominated by stirring despite the high  $Q_g$ .

### 3.3. Arc times and magnitudes

Variations in  $C_s$  between  $K_s/19$  and  $19K_s$  lead to significant variations in  $q_s$  in the range  $0.05 < q_s < 0.95$  applying Monod kinetics. Hence, in this range the regime RTDs alone provide limited insight in the  $q_s$  fluctuations that organisms are exposed to. Variations in  $q_s$  within a given regime can be described by registering the magnitude ( $\Omega_{s,max}$ ) and duration ( $\tau_{arc}$ ) of fluctuations compared to a reference value  $q_{ref}$  (Haringa et al., 2016), which constitutes the arc analysis method outlined in Section 2.1.2.

We set  $q_{ref}$  of  $q_s/q_{s,max} = 0.1$  for regime 2; this value is close to the regime median and is registered around the 2nd impeller from the top. Similar to the residence time analysis, a smoothed trajectory was used to decrease the sensitivity of  $\Omega_{s,max}$  to turbulent noise.  $\Omega_{s,max}$  is plotted as a function of  $\tau_{arc}$  in Fig. 6(A), showing markedly different behavior compared to the arc-analysis conducted in the *P. chrysogenum* case (Haringa et al., 2016), which is added for reference in Fig. 6(B).

This difference originates from the aforementioned compartmentalization (Section 3.1). Since  $C_s$  within a given circulation loop is reasonably homogeneous in the *S. cerevisiae* case, the duration of a trajectory within a single loop has no effect on  $\Omega_{s,max}$ ; only crossing over to a different loop leads to a jump in  $\Omega_{s,max}$  (Fig. 6(C)). In contrast, the intra-loop heterogeneity observed in the *P. chrysogenum* simulation means that longer trajectories lead to stronger extremes, even when confined to a single loop. This behavior is sketched in the right of Fig. 6(D).

Now, we focus on the *S. cerevisiae* case. Fig. 6(C) shows that  $q_s$  inside the upward loop emerging from the second impeller (center in Fig. 6(C)) is relatively homogeneous:  $q_s/q_{s,max} \approx 0.115$ . Most upward trajectories for lasting below 5 s are confined to this loop

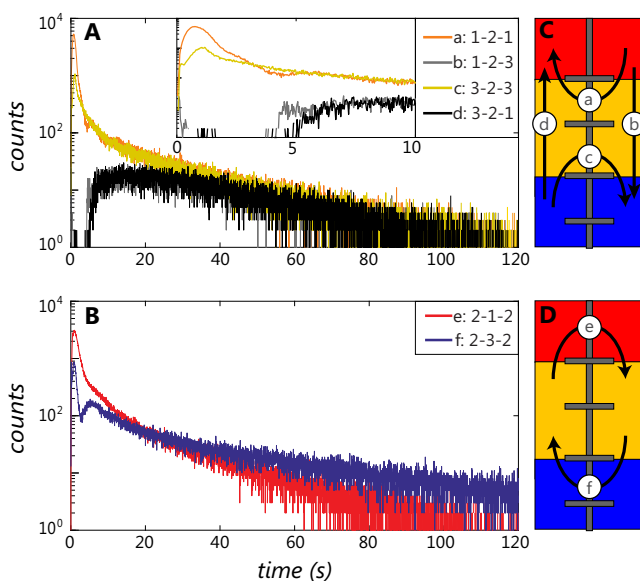


**Fig. 5.** Lin-log plot of the residence time distributions for the 6 different trajectories. (A) Trajectories through regime 2, discriminated by follow-up behavior (as indicated in (C)). (B) Trajectories through regime 1 and 3 (directions indicated in (D)). Mean residence times:  $\bar{\tau}_a$ : 6.96 s,  $\bar{\tau}_b$ : 38.37 s,  $\bar{\tau}_c$ : 14.03 s,  $\bar{\tau}_d$ : 39.41 s,  $\bar{\tau}_e$ : 8.03 s,  $\bar{\tau}_f$ : 34.19 s.

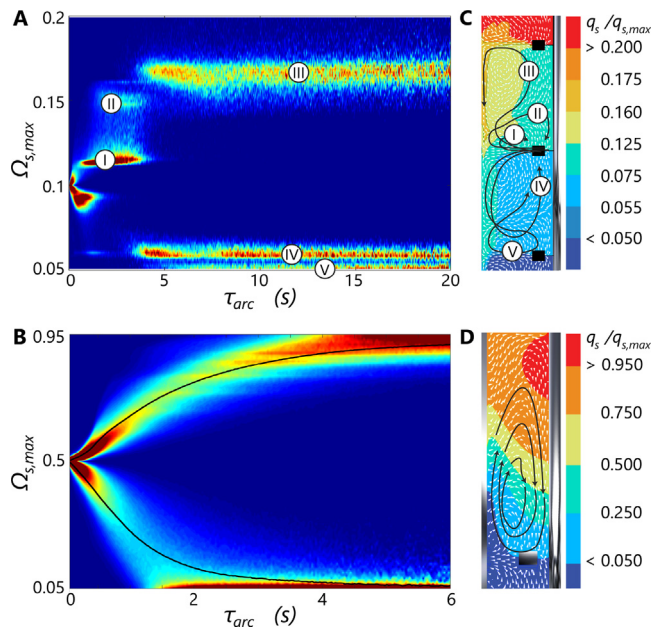


**Fig. 6.** Arc-magnitude analysis based on the method of Haringa et al. (2016).  $\Omega_{s,max}$  is the extreme value in  $q_s/q_{s,max}$  encountered over an arc trajectory. (A) Current case study, arc magnitude versus  $\tau_{arc}$  for regime 2. Each discrete level in (A) is associated with a certain circulation trajectories, marked by roman numerals, displayed in (C). (B) The *P. chrysogenum* case study of Haringa et al. (2016) (reproduced with permission), showing a smooth relation between arc magnitude and  $\tau_{arc}$ , explained by the trajectories shown in (D).

(type I trajectories), and consequently  $\Omega_{s,max} \approx 0.115$  is registered for nearly all upward trajectories with  $\tau_{arc} < 5$  s. No events with  $\Omega_{s,max} \approx 0.115$  are observed for  $\tau_{arc} > 5$  s meaning all trajectories following a single upward circulation are of shorter duration. For  $\tau_{arc} > 5$  s, a particle has either returned to the impeller (thus crossing  $q_{ref}$ ), or it has jumped to a higher circulation loop, which is referred to as a type III trajectory. Again, this circulation loop in itself is well mixed, meaning all particles on the type III trajectory register the same extreme,  $\Omega_{s,max} \approx 0.17$ .

Similar observations can be made in the downward direction, although only few trajectories with a duration  $\tau_{arc} < 5$  s are registered; by far most follow the type IV or V path, requiring at minimum 4 and 5 s, respectively, to return to  $q_{ref}$ . The observed duration is in good agreement with the per-loop circulation time estimated in Section 3.1. An oddity in this analysis are the type II trajectories which originate from the superimposed motion by gassing and the consequent asymmetry between the top- and bottom circulation loop around from the 2nd impeller from the top.

Like the per regime RTD, a distribution for  $\tau_{arc}$  can be constructed (Fig. 7(A)). For both up- and downward trajectories with respect to  $q_{ref}$  a multi-modal exponential decay is observed. The strong initial slope is associated with circulations in the direct vicinity of the impeller, the dip around  $t = 4$  s results from the lag-time associated with particles crossing over to different loops. Particles completing a single circulation in a second loop lead to a peak at  $t = 6$  s. For  $t > 10$  s there are many possible combinations of circulation trajectories, making it impossible to discriminate distinct modes and lag-times; their overall combination leads to a constant slope.

A similar plot can be constructed for regime 1, which is situated above the top impeller in its entirety. The regime 1 region encloses a single large circulation loop that gives a fixed slope for  $t > 5$  s, with some minor secondary loops due to gas flow leading to deviations for shorter times (Fig. 7(B)). An  $\Omega_{s,max}$  vs.  $\tau_{res}$ -plot for this regime is included in Appendix B for brevity.

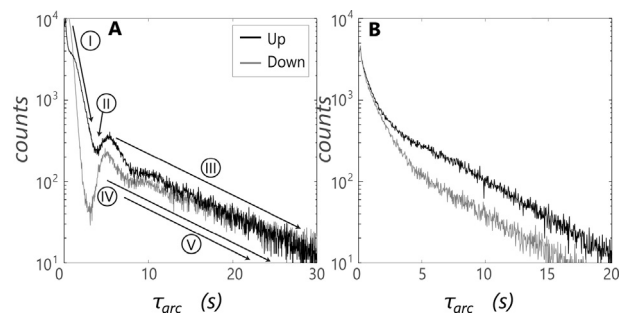


**Fig. 7.** (A) Distribution of  $\tau_{arc}$  for regime 2. The different peaks are associated with the circulation trajectories of Fig. 6 and indicated with the same roman numerals. (B) Distribution of  $\tau_{arc}$  for regime 1. (C) Arc magnitude versus  $\tau_{arc}$  for regime 1.

#### 4. Scale-down design

We now discuss possible scale-down simulator designs based directly on our CFD data, exploring both the multi-compartment and fluctuating-feed approach. There are significant challenges associated with designing a representative SD-simulator based on ideal unit operations (Haringa et al., 2016). These arise from the notion that in an ideal reactor, the rate of change in substrate concentration ( $dC_s/dt$ ) experienced by a micro-organism depends solely on the consumption rate  $q_s$ , which reads  $dC_s/dt = C_x \cdot q_s$ . In non-ideal reactors, the rate-of-change experienced by organisms is governed both by consumption and local mixing between glucose-rich and glucose-lean fluid elements:  $dC_s/dt = C_x \cdot q_s \pm [mixing]$ . For organisms coming from a glucose-rich zone, mixing results in  $dC_s/dt > C_x \cdot q_s$ , due to the interaction with glucose-lean broth.

The implication of this observation is best illustrated by analyzing the type *b* trajectory (Fig. 5), which has a mean residence time  $\bar{\tau}_b = 40$  s. Changing from  $q_s/q_{s,max} = 0.2$  to  $q_s/q_{s,max} = 0.05$  by consumption alone requires 67 s when  $C_x = 10$  g/L, hence,  $\bar{\tau}_b$  cannot be replicated in an ideal SD-simulator operating at the industrial biomass concentration  $C_x = 10$  g/L. In a 2-vessel setup, the same effect constrains the concentration ratio  $C_{s,2}/C_{s,1}$  between the vessels. Assuming 1st order kinetics and a feed in vessel 1, for example, gives  $C_2 = C_1/(1 + k \cdot \tau_2)$ .

In Haringa et al. (2016) these issues were regarded as prohibitive for a representative SD simulation due to the very high industrial  $C_x$  and very rapid  $q_s$ -variations encountered in the *P. chrysogenum* case study. With the current *S. cerevisiae* setup, representative scale-down is feasible. First, the industrial  $C_x$  is lower, leaving some room for variation: setting  $C_x = 16.7$  g/L is sufficient to replicate  $\bar{\tau}_b$ . We apply  $C_x = 20$  gm/L here to leave some headroom. Second, in terms of operation, the high  $\tau_{circ}$  and more favorable rheology should allow for multi-compartment replication without running into pumping or mass transfer problems.

##### 4.1. 3-compartment approach

First, we propose a design for a 3 compartment SD simulator. Any type of SD-simulator based on (ideal) lab reactors has a total of 5 degrees of freedom (Noorman, 2011):

- Number of compartments  $N_V$
- Vessel volumes  $V_i$
- Flow patterns
- Circulation rates  $\phi_i$
- Feed rates  $F_i$  (and locations)

By choice we fixed  $N_V = 3$ , each compartment representing one of the regimes discussed in Section 3.2. The residence time distri-

butions clearly show that each regime is best represented by a stirred tank, which under ideal assumptions has an RTD following from Eq. (6), with  $\tau_i = V_i/\phi_i$  where  $\phi_i$  is the compartment flowrate.

$$f(t) = \frac{1}{\tau_i} \exp(-t/\tau_i) \quad (6)$$

The compartment volume  $V_i$  follows from the volumetric regime distribution, reported in Table 2, column 2. All values are given per liter of total volume; the total volume can be freely chosen provided the ideal mixing assumption is met. The flowrates  $\phi_i$  cannot be calculated directly from  $\bar{\tau}_i$  (Fig. 5) as  $\phi_1 + \phi_3 \neq \phi_2$ , violating mass conservation. A reconciliation step is required to determine which set of vessel residence times  $\tau_i$  best replicates the CFD distributions, constrained by  $\phi_1 + \phi_3 = \phi_2$ . The feed rate  $F_i$  is calculated from the desired operating concentration per vessel, which is set volume-averaged uptake rate,  $\bar{q}_s/q_{s,max}$ . This average was determined from the Eulerian  $q_s/q_{s,max}$  distribution (Fig. 4); the values are reported in Table 2. To keep the design simple, we do not consider superimposed variations in  $q_s/q_{s,max}$  by varying the feed, which could be based on the arc-behavior of Section 3.3.

To reconcile  $\phi_i$ , constrained minimization is performed in MATLAB, using the sum of squares of all residence time distributions over all  $N_t$  time intervals (Eq. (7)) as a cost function:

$$cost = \sum_{i=1}^3 (\sum_{j=N_t}^{RTD(j)} (RTD(j) - f(j))^2)_i \quad (7)$$

since we use a single vessel to fit regime 2, the four RTDs for the individual trajectories through this regime were summed into a single distribution for fitting purposes. The best fit, named design M1, is summarized in Table 3. A low  $\tau_i$  is reported for each compartment due to the short-timescale variations dominating the fit. This outcome is undesirable since the long-timescale variations, which typically have a higher amplitude, are expected to have a stronger impact on the organism. In design M1, the frequency of such events is strongly underestimated. A more practical issue is that the short  $\tau_i$  means that the target  $\bar{q}_s/q_{s,max}$  cannot be met, due to the reasons outlined in Section 4.

For an improved design (M2), also reported in Table 3, the RTDs were fitting only to the interval  $20 \text{ s} < t < 60 \text{ s}$ . The overall  $R^2$  of this fit is clearly worse, due to the underestimation of the short-timescale events. However, the RTD shows a more satisfactory reproduction of long-term behavior (Fig. 8(A)) as the design filters out brief, low amplitude substrate fluctuations while retaining the desired long-term behavior (see Fig. 9).

The feed rate can subsequently be computed from the per-vessel species balance. We propose to operate the SD-simulator as a chemostat with constant  $C_x$ . Under chemostat conditions, the growth rate ( $\mu$ ) by definition equals the dilution rate ( $D_r$ ), while  $C_s$  is variable. To fix  $C_s$  (and  $q_s$ ) at the proposed target values,  $\mu$  must be estimated under the simulated conditions, and  $D_r$  must be set accordingly. Assuming that variations in  $\mu$  are slow compared to imposed extra-cellular variations, we assume  $\bar{\mu} = f(\bar{q}_s)$ . This assumption supported by the work of Suarez-Mendez et al. (2014) and Suarez-Mendez (2013), who showed that variations in metabolites such as amino-acids and TCA intermediates are strongly dampened when 400 s feast-famine cycles are imposed. It is likely variations in a complex process such as growth, requir-

**Table 2**

Design aims for the 3-compartment scale-down approach.  $V$  is fixed,  $q_s/q_{s,max}$  is based on the per-regime mean uptake rate.

| Vessel | $V$ L/L | $q_s/q_{s,max}$ |
|--------|---------|-----------------|
| T1     | 0.24    | 0.309           |
| T2     | 0.41    | 0.105           |
| T3     | 0.35    | 0.034           |

**Table 3**

Tank specifications for design M1 (top three rows) and design M2 (bottom three rows).

| Vessel | $\phi_i$ L/L/s | $\tau_i$ | $R^2$ |
|--------|----------------|----------|-------|
| T1-M1  | 0.0663         | 3.62     | 0.80  |
| T2-M1  | 0.097          | 4.23     | 0.68  |
| T3-M1  | 0.0307         | 11.41    | 0.67  |
| T1-M2  | 0.0093         | 25.8     | 0.31  |
| T2-M2  | 0.0193         | 21.2     | 0.29  |
| T3-M2  | 0.0100         | 34.9     | 0.54  |

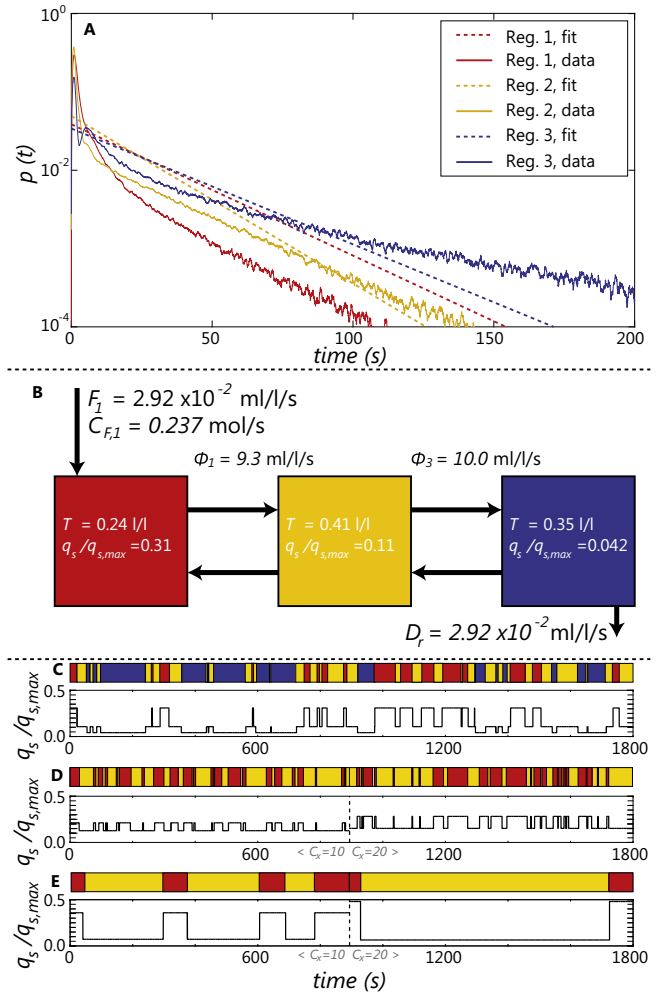


**Fig. 8.** (A, B) Specifications design M2. (A) Comparison between the normalized RTDs from CFD (solid) and fitted RTDs (dashed). (B) Schematic design of the proposed simulator. Volumes and flow rates are given per liter of total setup volume; the absolute vessel size is a free parameter. (C–E) Oscillation profiles for three multi-vessel approaches as experienced by a single organism circulating through the system. (C) Design M2, current work.  $C_x = 20$  g/L. (D) Sweere et al.,  $\tau_{circ} = 36$  s,  $C_x = 10$  g/L (left) and  $C_x = 20$  g/L (right). (E) Sweere et al.,  $\tau_{circ} = 338$  s,  $C_x = 10$  g/L (left) and  $C_x = 20$  g/L (right).

ing such intermediates, are consequently dampened as well. This does not imply that  $\bar{\mu}$  under dynamic conditions equals  $\bar{\mu}$  under steady conditions with the same  $\bar{q}_s$ , but lacking data on the effect of  $q_s$ -dynamics on  $\bar{\mu}$ , we here do assume that  $\bar{\mu}$  can be estimated by solving the Herbert-Pirt equation, Eq. (8):

$$\bar{\mu} = (\bar{q}_s - m_s) \cdot Y_{sx} \quad (8)$$

where the maintenance coefficient  $m_s = 0.01$  gm<sub>s</sub>gm<sub>dw</sub>/h and  $Y_{sx} = 0.5$  (Postma et al., 1989a; Pham et al., 1998). The CFD

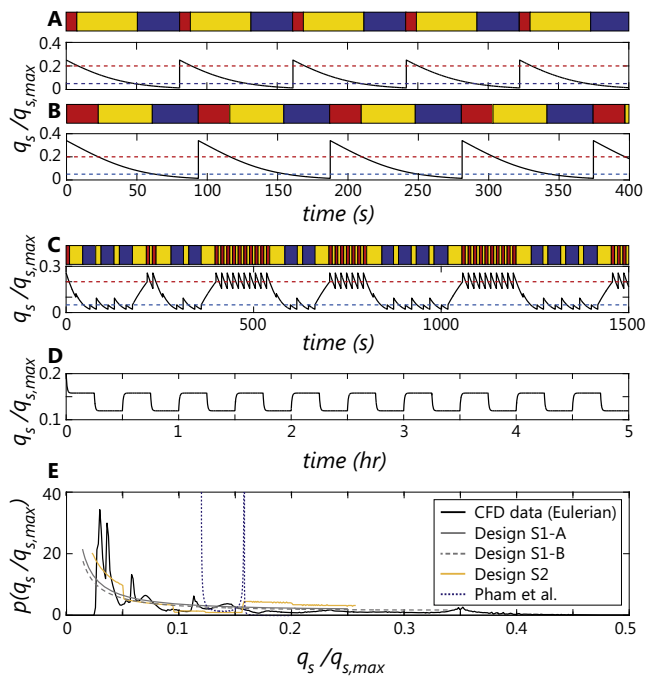


**Fig. 9.** Design strategies for a single-vessel SD-simulator. (A, B) Block-based design and  $q_s/q_{s,max}$  vs.  $t$  series for design S1-A and S1-B of Table 5, respectively. (C) Randomized feed signal (design S2), based on  $\bar{\tau}$  for each regime. (D) Oscillation pattern of Pham et al.,  $C_x = 10$  gm/L (E) overlays the volumetric  $q_s$ -distribution for a 300 h stretch of such a signal, compared with the (Eulerian)  $q_s$ -distribution of the CFD data.

simulations give  $\bar{q}_s = 0.129q_{s,max}$ , yielding  $\bar{\mu} = 0.10$  1/h, or  $D_r = 2.8 \cdot 10^{-5}$  L/L/s. If an instantaneous adaptation of  $\mu$  to the conditions in each individual compartment is assumed instead, the result setup-average  $\bar{\mu} = 0.11$  1/h and  $D_r = 3.1 \cdot 10^{-5}$  L/L/s, showing that there comparatively little difference between these estimations of  $D_r$ .

Calculating the feed rate  $F_i$  and feed concentration  $C_{f,i}$  requires solving the coupled mass balances within an optimization routine, where the sum of individual vessel feeds is constrained:  $\sum^{i=3} F_i = D_r = 2.8 \cdot 10^{-5}$  L/L/s. Optimization was conducted using the genetic algorithm available in MATLAB, yielding the feed parameters reported in Table 4 for design M2; the design is outlined graphically in Fig. 8(B). An organism lifeline to exemplify how a single organism might experience the conditions this design is shown in Fig. 8(C). As noted before, the feed and concentration constraints could not be satisfied for design M1 with  $C_x = 20$  gm/L.

When designing a fed batch system rather than a chemostat, a reasonable choice may be to regard the above conditions as a starting point, subsequently allowing  $C_x$  to develop freely while keeping the feed constant. Ideally,  $\phi_i$  and  $V_i$  should change over time to reflect the changes in regime distribution inside the industrial reactor over time, which can be estimated by repeating the CFD analysis for different  $C_x$ .

**Table 4**  
Design M2: Best fit for the feed conditions and estimated per-Compartment glucose uptake rate.

| Vessel | $c_f$ mol/L | $F_i$ 1/s           | $Q_{s,fit}$ |
|--------|-------------|---------------------|-------------|
| T1-M2  | 0.25        | $2.8 \cdot 10^{-5}$ | 0.309       |
| T2-M2  | 0.041       | $5.2 \cdot 10^{-8}$ | 0.107       |
| T3-M2  | 0.021       | $4.5 \cdot 10^{-8}$ | 0.042       |

## 4.2. Single vessel approach

Next, we describe how a single vessel, varying feed simulator can be designed. The feed rate is the only degree of freedom in this approach, having the advantage of being significantly easier to operate, especially for high  $C_x$  and short  $\tau_{circ}$ .

The simplest oscillating feed approach imposes a glucose pulse at  $t = 0$  of each cycle, followed by a consumption-only phase; this is typically called a feed-famine approach (used by e.g. de Jonge et al., 2011; van Kleeff et al., 1996; Suarez-Mendez et al., 2014). Using the terminology applied in Fig. 5, this approach follows an  $e - b - f$  trajectory. The most straightforward cycle (design S1-A) replicates the per-trajectory mean residence time,  $\tau_e = 8.03$  s,  $\tau_b = 38.37$  s,  $\tau_f = 34.19$  s. Design S1-A restricts  $C_x$  at 16.7 g/L, since a higher  $C_x$  increases the consumption rate, decreasing  $\tau_i$ . This restriction constrains  $q_s$  during the feed phase to  $0.25q_{s,max}$ ; we refer to this maximum in  $q_s$  as  $QM$ . All design parameters are summarized in Table 5.

While design S1-A replicates the mean residence times for this particular trajectory, but the overall regime division is off (mainly for regime 1) and  $\bar{q}_s/q_{s,max}$  is too low and. Increasing  $\tau_e$  and  $\tau_f$ , in order to abide the total regime distribution, yields design S1-B reported in Table 5. This design simultaneously improves the agreement in  $QM$ , at the cost of reducing the agreement in  $\tau_e$ . The S1 designs are outlined graphically in Fig. 8(A) and (B), respectively. Both S1-designs do not capture regime follow-up properly, as trajectories  $a$ ,  $c$ ,  $d$  are ignored.

**Randomized cycle design** The above designs have their merits in studying how organisms respond to repetitive, well-defined variations, with a duration of the correct order-of-magnitude. Yet, they do not include several aspects of the CFD results and an alternative design including regime follow-up and properly capturing residence time distribution in each regime must be considered. Here, we propose a randomized cycle design which captures the regime follow-up behavior and  $\bar{\tau}_i$  for each regime; capturing the full RTDs is problematic due to the ‘consumption-only’ limitation discussed in Section 4, and is considered to be out of the current scope.

A randomized  $q_s/q_{s,max}$  profile from 6 building blocks, each representing one of the transition trajectories reported in Fig. 5, with an associate block duration equal to  $\bar{\tau}_i$ . After each  $e$ - or  $f$ -type block, a random number generator is used to determine which block type follows based on the follow-up distribution. In this design, rather than feeding a single pulse at  $t = 0$  of a cycle, more complex feed profiles will arise. Therefore, we do not limit the biomass concentration to  $C_x = 16.7$  g/L but, as for the 3-vessel design, use  $C_x = 20$  g/L. In the  $e$ - and  $f$ -type block a small glucose pulse is administered halfway, to retain a block duration equal to  $\bar{\tau}_i$ . In the type  $d$ -type block, the substrate concentration is gradually increased. Type  $a$  and  $c$  blocks both have a feed-spike at the start of the block, with consumption only during the remainder. An example of a sampled  $q_s/q_{s,max}$ -signal based on the approach outlined above is displayed in Fig. 8(C).

Running the cycle for  $t = 300$  h yields a regime division of 19%, 43%, 38% for regimes 1, 2, 3, respectively, reflecting the Lagrangian distribution reported in Section 3.2. The average uptake  $\bar{q}_s/q_{s,max} = 0.110$ , in excellent agreement with the Lagrangian and acceptable agreement with the Eulerian CFD results. A weak design aspect is the achieved  $QM = 0.26$ , a consequence of the short duration of the type- $e$  block. This can be improved by further increasing  $C_x$  or by including the block RTD, allowing longer exposures. Considering the overall feed rate under chemostat conditions, the calculations are equal to the 3-vessel design.

**Distributions of  $q_s/q_{s,max}$**  The time-averaged  $q_s$ -exposure distribution is captured in Fig. 8, E for each proposed feed cycle, and compared with the Eulerian distribution observed in the CFD sim-

**Table 5**

Simple single vessel design strategies, based on the global regime distribution, compared to the Eulerian and Lagrangian simulation perspective (row 1 and 2, respectively). Design S1-A and B consider single-pulse feeding strategies, S2 a more complex oscillation strategy. R1, R2, R3 are the regime fractions per regime.

| Design  | $\tau_a$<br>[s] | $\tau_b$<br>[s] | $\tau_c$<br>[s] | $\tau_d$<br>[s] | $\tau_e$<br>[s] | $\tau_f$<br>[s] | $\tau_{cycle}$<br>[s] | R1<br>[%] | R2<br>[%] | R3<br>[%] | QM<br>– | $q_s/q_{s,max}$<br>– |
|---------|-----------------|-----------------|-----------------|-----------------|-----------------|-----------------|-----------------------|-----------|-----------|-----------|---------|----------------------|
| CFD (E) | –               | –               | –               | –               | –               | –               | n/a                   | 24        | 41        | 35        | 0.66    | 0.129                |
| CFD (L) | 7.0             | 38.4            | 14.0            | 39.4            | 8.0             | 34.2            | n/a                   | 18        | 42        | 40        | 0.66    | 0.11                 |
| S1-A    | –               | 38.4            | –               | –               | 8.0             | 34.2            | 80.6                  | 10        | 48        | 42        | 0.25    | 0.091                |
| S1-B    | –               | 38.4            | –               | –               | 22.50           | 32.8            | 93.7                  | 24        | 41        | 35        | 0.34    | 0.123                |
| S2      | 7.0             | 38.4            | 14.0            | 39.4            | 8.0             | 34.2            | n/a                   | 19        | 43        | 38        | 0.26    | 0.11                 |

ulation. Naturally, the compartment peaks are not resolved by any design, but the global trends are retrieved, most properly by S2. S1-A and S1-B only roughly capture the global distribution, with S1-B performing better in the high-end region. The highest values of  $q_s$  are poorly captured by design S2, which is compensated in the range  $q_s/q_{s,max} = 0.2–0.25$ . A deficit in counts in the region of  $q_s/q_{s,max} = 0.1–0.15$  is visible as this region lies outside of the current range for both the *a* and *c*-block; this can be fixed by either increasing  $C_x$ , or accounting for the RTDs.

#### 4.3. Previous SD experiments for *S. cerevisiae*

Previously, scale-down studies on *S. cerevisiae* have been performed replicating both oxygen (Sweere et al., 1988a; Sweere et al., 1988c; Abel et al., 1994) and glucose gradients (George et al., 1993, 1998; van Kleeff et al., 1996; Pham et al., 1998; Sweere et al., 1988d; Suarez-Mendez et al., 2014; Heins et al., 2015). Being the focus of the current work, we briefly discuss the glucose-variation experiments.

*Multi-compartment* George et al. (1993, 1998) based their scale-down study on a 215 m<sup>3</sup> industrial bubble column, with a PFR representing the ‘crabtree compartment’ ( $C_s > 0.11$  gm/L for the used strain), which contained 10% of the process volume. Despite replicating a different reactor, this volume was based on observations by Larsson et al. (1996).  $C_x$  was 10–50 g/L, in the industrial range. Both the SD-simulator and the well mixed benchmark of George et al. ran at high residual substrate (glucose + fructose) concentrations, between 100 and 150 mg/L most of the time. These levels roughly correspond to experimental samples taken at heights of 2.1 and 6.3 m in their fermentor. With a total filled 9.7–16.3 m, the overall gradient was likely stronger. The average residence time in the stirred compartment was 9 min, the PFR residence time 1 min. The mixing time in a bubble column can be estimated using Eq. (9) (van der Lans and van’t Riet, 2011), yielding  $\tau_{95} = 46$  s, with  $\tau_{circ}$  around a factor 4 lower. This indicates that the SD-simulator design of George et al. strongly overestimated the fluctuation duration.

$$t_m = 1.6T^{2/3} \cdot (gU_g)^{-1/3} \quad (9)$$

Based on our CFD data, the inclusion of feed variations is a simple upgrade that can be proposed for the design of George et al. This would lead to a  $q_s$ -profile similar to Fig. 8(C), where the longest oscillations act at timescales of several minutes, with more rapid substrate variations being superimposed. Such a hybrid between the varying feed and multiple vessel approach can reproduce variations at the relevant timescales, while keeping  $\tau_{circ}$  for individual vessels in the range utilized by George et al.

Sweere et al. (1988d) simulated glucose variations in a 2 STR system with  $\tau_{circ}$  ranging between 0.6 and 20.5 min, using strain CBS8066. They observed a reduction in  $C_x$  and increase in ethanol production for increasing  $\tau_{circ}$ . This is likely an effect caused by the increasing gap in residual  $C_s$  upon increasing  $\tau_{circ}$ , which is reflected in the growing difference in the respiration quotient

between the two compartments while increasing  $\tau_{circ}$ . Overall,  $C_x$  varied between 6.5 and 25 g/L during the process. No information on  $C_s$  was provided, but an estimate could be made by assuming Monod kinetics. From the microbial point of view, this yields  $q_s$  profiles as given in Fig. 8(D) and (E), for  $\tau_{circ} = 0.6$  min and  $\tau_{circ} = 6.3$  min, respectively. For both cases, the profiles at  $C_x = 10$  g/L and  $C_x = 20$  g/L are shown (left and right of the dashed line respectively).

Fig. 8(D) and (E) shows that  $q_s$  oscillates between regimes 1 and 2, but the oscillation magnitude depends strongly on  $\tau_{circ}$ ; ranging from 0.13 to 0.21 (with negligible ethanol production) for  $C_x = 10$  g/L and  $\tau_{circ} = 0.6$  to  $q_s/q_{s,max} = 0.06–0.48$  in case  $\tau_{circ} = 6.3$  min and  $C_x = 20$  g/L. The latter conditions reflect the magnitude of industrial fluctuations better, while  $\tau_{circ} = 0.6$  mimics their duration best. Overall, the work of Sweere et al. covers cases that provide a decent reflection of industrial frequencies (for low  $\tau_{circ}$ ) and amplitude (for high  $\tau_{circ}$ ).

The two-compartment chemostat of Heins et al. (2015) operated at  $C_x = 10–20$  g/L, representing part of an industrial operation. The circulation time  $\tau_{circ} = 1.17$  h at minimum, hence the exposure of organisms to extra-cellular variations is not considered to be truly industrially representative. One of the merits of this setup is the strong  $C_s$  gradient between the vessels ( $C_s \gg 1$  g/L in compartment 1, and  $C_s \ll 1$  g/L in compartment 2), allowing to study the effect substrate concentration variations with an extreme magnitude on the population.

*Single-compartment:* Pham et al. (1998) used a fluctuating feed experiment to validate their metabolic model for CBS8066, imposing oscillations of 15% around the mean substrate feed rate of 21 gm/h in a fed batch process. Both  $C_x$  and the filled reactor volume are dynamic; for comparison we constructed a snapshot where  $C_x = 10$  g/L and  $V \approx 9$  L ( $C_x = 20$  g/L was not reached experimentally). No ethanol production is predicted to occur under these conditions as  $q_s/q_{s,max}$  oscillates between 0.12 and 0.158 (Fig. 8(D)). Their experimental data confirms the lack of ethanol production. Compared to our CFD benchmark, it is clear that the oscillations imposed by Pham et al. were too long in duration and too low in magnitude to be considered industrially representative.

van Kleeff et al. (1996) exposed strain CBS8066 to feast famine cycles. The cycle duration was 200 s or 400 s, with a feed period of 20 and 40 s, respectively. The dilution rate was approximately  $D_r = 0.055$  1/h and  $C_x$  was around 3.6 g/L. Inspired by van Kleeff et al., Suarez-Mendez et al. (2014) imposed 400 s cycles (40 s feed) to strain CEN PK 113-7D, with  $C_s$  oscillating between 0.46 and 0.094 mmol/L at  $C_x = 3.46$ . A 5% reduction in  $C_x$  compared was observed compared to their steady state reference, without ethanol production. For illustrative purposes, we assume the uptake kinetics of CBS8066 apply to CEN PK 113-7D, in which case  $q_s$  cycled between 0.048 and 0.082  $q_{s,max}$ . Both for van Kleeff et al. and Suarez-Mendez et al., the long cycle times and low fluctuation magnitude (due to the low  $C_x$ ) indicate their setups are not industrially representative. Of course, they are suitable for revealing the effects of well-defined, repeatable fluctuations on micro-organisms.

#### 4.4. Towards representative scale-down

Above, relatively simple SD-designs were discussed, which can all be realized within current scale-down practices. Only design S2 is of a type not currently employed. Our design approach currently focused on reproducing the fluctuation duration, and the proposed designs are somewhat weaker in capturing the fluctuation magnitude. Of course, one can opt to reduce the agreement in duration in order to increase the agreement in magnitude: this trade-off between duration and magnitude applies to any ideal scale-down simulator, although its severity depends strongly on  $C_x$ . If possible, the balance between magnitude and duration should be decided based on which of the two most influences the organism; to perform such an analysis, information on the metabolic response of the organism is of course required. Within the stated limitations, the current CFD-based scale-down proposals are a reasonable reflection of the industrial scale conditions and are a step forward compared to the current generation of scale-down simulators which were typically designed based on a combination of global parameters such as  $\tau_{95}$  and intuition, often leading to an overestimation of the fluctuation duration and/or an underestimation of the amplitude.

The CFD data suggests considering more complex designs than were proposed, these were currently considered to be out of scope. More complex designs may include, for example, superimposing the intra-regime variations (discussed in Section 3.3) to yield better agreement with the overall glucose distribution (Fig. 3). For example, the  $q_s$ -profile of design S2 (Fig. 8(C)) inspires a 2-stirred tank design with relatively long residence times, with superimposed feed oscillations covering more rapid dynamics. More complex one-vessel designs may include sampling of the RTDs rather than using  $\bar{\tau}_i$ , to more faithfully reproduce the spread fluctuation durations in a stirred tank, provided this sampling can be reconciled with the limitations discussed at the start of this section. More complex scale-down designs, and ranking of the designs in terms of their industrial representative qualities, will be the subject of future work.

#### 5. Concluding remarks

In this work we simulated a stirred 22 m<sup>3</sup> *S.cerevisiae* fermentation, containing a large scale substrate concentration gradient due to the competition between mixing and substrate uptake. Good agreement was observed in terms of power number and gas holdup, and reasonable agreement was obtained for  $k_{la}$  and the mixing time. Experimentally, the glucose concentration was sampled at three locations; the agreement between the experimental and simulated concentrations was decent considering the inherent assumptions made in the simulation approach. The observed concentration gradient is strongly compartmentalized, with substrate being well mixed within individual circulation loops originating from the individual Rushton impellers, while heterogeneity is observed between the loops.

We used Euler-Lagrange CFD to study the concentration variations as experienced by micro-organisms. Inspired by (Noorman, 2011), the vessel was divided in three virtual regions: ethanol producing/glucose consuming (regime 1), glucose consuming (regime 2) and low glucose uptake (regime 3). Based on the analysis methodology presented in Haringa et al. (2016), the residence time distribution in each regime was determined, as well as statistics describing the magnitude and duration of concentration fluctuations within each regime. In line with the observed compartmentalization, the relation between the fluctuation duration and magnitude showcased discrete behavior, associated with the different circulation loops in the reactor.

Scale-down simulators, lab scale setups that reproduce temporal variations in the extra-cellular environment, were designed based on these fluctuation statistics originating from our CFD analysis. These designs employ both on the fluctuating feed and multiple compartment approach. Three feed strategies of varying complexity are proposed, and one 3-compartment design is put forward. They provide a reasonably faithful reproduction of the large scale substrate concentration variations observed in the CFD data, although operational constraints prohibit capturing the most rapid oscillation events. All designs are feasible to operate currently applied scale-down equipment. To conclude, we conducted an analysis of previously operated scale-down simulators for *S. cerevisiae* which shows that, with the hindsight offered by state-of-the-art CFD simulations, most do not closely represent industrial conditions. With the availability of novel (CFD) methodologies, improvements to these designs that improve their agreement with industrial conditions can be proposed.

#### Acknowledgments

We want to thank our colleagues at ECUST Shanghai, DSM and DSM Sinochem pharmaceuticals and the DSM biotechnology center for our fruitful collaboration. Thanks go to Dr. Walter van Gulik and Prof. Ju Chu for hosting discussions and exchanges between the different project partners and Prof. J.J. Heijnen, Prof. Matthias Reuss and Özgür Gunyöl for their insights. Students Harm Gerlings, Laurens Tijsseling and Marenka Brussee contributed to the simulation work. This work has been conducted within a multi-party research project, between DSM-Sinochem Pharmaceuticals, TU Delft, East China University of Science and Technology and Guojia, subsidized by NWO and MoST (NWO-MoST Joint program 2013DFG32630). All sponsors are gratefully acknowledged.

#### Appendix A. Additional simulation details

##### A.1. Simulation setup

Due to the highly coupled, non-linear nature of the simulation and challenges associated with particle tracking, the simulation was conducted in several stages to ensure stability. This appendix provides a brief treatment of the overall workflow and encountered issues.

*Eulerian flow fields - pressure outlet.* First, the two-phase flow was solved in the domain with a full headspace, using a steady state solver. A pressure outlet (PO) boundary condition (gas backflow) was prescribed at the top. This was preferred over a degassing condition to allow for expansion of the broth volume. In contrast, a degassing boundary condition fixes the total filled (gas + liquid) volume, leading to variations in liquid volume as a consequence of changes in gas holdup.

However, the liquid mass was not conserved during the steady state simulation with either boundary condition, as a consequence of the residual terms in the mass balance: these resulted in a small liquid mass increase over the iterations. Hence, we first converged the flowfield while allowing liquid mass to increase and subsequently patched the top of the domain with 100% gas such that the initial liquid mass was recovered. An additional 1500 iterations were subsequently executed to converge the simulation (residuals  $\approx 10^{-4}$  and  $\bar{U}_{liq}$ ,  $\bar{d}_b$  stable within 2.5%) Deeper convergence could not be reached, both in steady state and transient mode. Running the simulation fully in a transient solver did reduce mass-imbalances, but the approach applied here (first reaching crude convergence, despite the imbalances) proved significantly faster.

After convergence, the gas-fraction field and bubble size were frozen, executing an additional 500 iterations for turbulence and

momentum only, yielding velocity residuals of  $\approx 10^{-4}$ , a continuity residual  $< 10^{-5}$  and  $\overline{U}_{liq}$  stable within 2%. This was deemed satisfactory convergence, being well in line with earlier simulations of the same system (Gunyol et al., 2009). After convergence, the top was cut off at the free surface height, prescribing a degassing boundary condition at the new top face. This change in boundary condition was required to prevent particles from getting stuck in the headspace during later simulation stages. An additional 4000 iterations were executed to re-converge the flow at the top. The residuals for all equations except bubble size were  $\approx 10^{-4}$ , for bubble size a residual value of  $\approx 3 \cdot 10^{-3}$  was achieved. Here,  $\overline{U}_{liq}$ ,  $\overline{\alpha}$ ,  $\overline{d}_b$  all were stable within 2.5%. Gas backflow over the degassing boundary was responsible for the formation of a small ‘vortex’ around the shaft (visible in Fig. 2 of the main text), where the gas fraction was elevated. It was not possible to avoid this behavior (increasing the run-time would increase the gas fraction).

**Mixing and reaction.** During the mixing stage, the flow equations (turbulence, momentum, volume fraction and bubble size) were disabled, fixing their respective fields. The simulation was switched to transient mode ( $\Delta t = 0.01$  s) and tracer was added as a patch at the location  $[r$  (m),  $Y$  (m),  $\theta$  (deg)] = [0.31, 6.48, -5] with  $\theta = 0$  being the baffle plane. Tracer response curves were registered at  $r = 0.83$  m,  $\theta = 15$  deg and (bottom to top)  $Y = 1.12$ , 4.04, 6.56 m. To study the Lagrangian mixing behavior, 5,750,000 particles were released at the same feed location, and the number of particles was registered in each probe-containing grid cell. The timestep size was  $\Delta t = 0.002$  s during particle tracking, this value was chosen to prevent particles from getting stuck in the trailing vortices. The Lagrangian data was smoothed over 4 s to remove noise due to the limited number of particles per grid-cell ( $O(10)$ ). A sensitivity analysis regarding the influence of the smoothing window is presented in Fig. A1, showing that for a smoothing window of 4+ s the results are insensitive to the window size, while for smaller windows noise significantly affects the mixing time.

After completing the mixing stage, the concentration gradient was resolved in steady state, keeping all equations except species transport frozen. Monod kinetics were included via a volumetric reaction user-defined function (UDF). Glucose was fed via source terms in a small region centered at  $[r$  (m),  $Y$  (m),  $\theta$  (deg)] = [0.30, 7.44, 0], mimicking a feed entering via the free surface. Once the steady-state concentration gradient was resolved, the simulation was switched back to transient and particles were added for lifeline registration.

**Lifeline registration.** A total of 12,500 particles were tracked during the lifeline collection stage, with a timestep size  $\Delta t = 0.005$  s; larger timestep sizes led to particles getting stuck in the trailing vortices. The observed instantaneous extra-cellular glucose concentration  $C_s$  was registered for each particle with a registration

interval of 0.03 s using a user-defined function. The data for all timesteps was re-ordered in MATLAB to form a set of  $C_s$  versus  $t$  series which were subsequently analyzed. An example of three raw particle tracks is given in Fig. A2. The timestep size of 0.03 s was set to be significantly shorter than the circulation time inside individual circulation loops (which is  $\approx 5$  s), to ensure even the shortest trajectories inside each loop were properly resolved. An additional consideration is that the timestep size should be much smaller than the timescale  $\tau_{rxn}$  representative of the fastest reaction included in the applied metabolic model, which is easily achieved in this case.

## A.2. Detailed mixing analysis

Experimental mixing times of 147 s (Noorman, 2011) and 166 s (Vrábel et al., 1999) are reported experimentally for the studied fermentation process. Besides the mixing times, an experimental probe response curve is available from the data of Noorman for the bottom probe. The simulated tracer response for each of the three installed probes is given in Fig. A3, for every employed simulation approach. Employing a pressure outlet boundary condition combined with a turbulent Schmidt number  $Sc_T = 0.7$  yields good agreement with the experimental  $\tau_{95}$  of Vrábel.

All other simulation approaches yield a higher  $\tau_{95}$ , which was unexpected; no major differences were expected upon changing the boundary condition, and reducing  $Sc_T$  typically reduces  $\tau_{95}$  (Montante et al., 2005; Gunyol et al., 2009; Delafosse et al., 2014; Haringa et al., 2016). These observations were attributed to mass imbalances that were observed over time in the simulations. They were to some extent present in all Eulerian cases; this is evident from the variations in the integral tracer mass fraction  $Y_s$ , reported in Fig. A3(B).

These imbalances, like the total water mass imbalance discussed above, result from the nonzero momentum residuals. When freezing the flowfield, the sum of residuals is nonzero, yielding some accumulation of tracer during each timestep, which is most pronounced in the first timesteps when the local gradients are strong. Although this effect happens in single phase simulations, too, the residuals in those simulations ( $\approx 10^{-6}$ ) are typically small enough to yield negligible accumulation within the time-frame  $\tau_{mix}$ . The strong non-linearity of the current problem results in higher residual values ( $\approx 10^{-4}$ ), that are acceptable for the flow pattern and holdup, but do lead to a non-negligible tracer variation during mixing. If the goal is to assess the  $\tau_{mix}$  with great accuracy, it is therefore not recommended to freeze the flow-fields, despite the considerable difference in computation time. In case of the Lagrangian mixing simulation,  $\tau_{95} = 183$  s was recorded. As discussed in the main text, this value was deemed most accurate as the Lagrangian approach does not suffer from mass accumulation, and the number of particles was conserved perfectly.

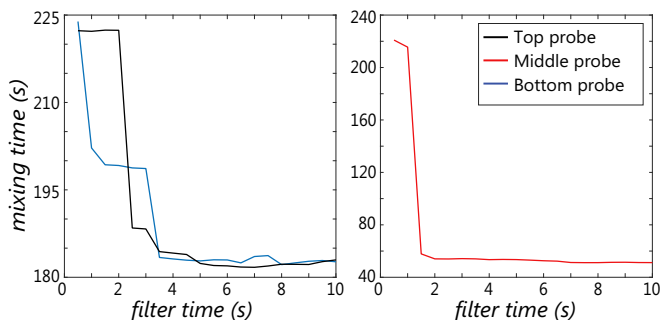


Fig. A1. Sensitivity of Lagrangian mixing time to the applied moving-average window time. (A) Top and bottom probe. (B) Middle probe.

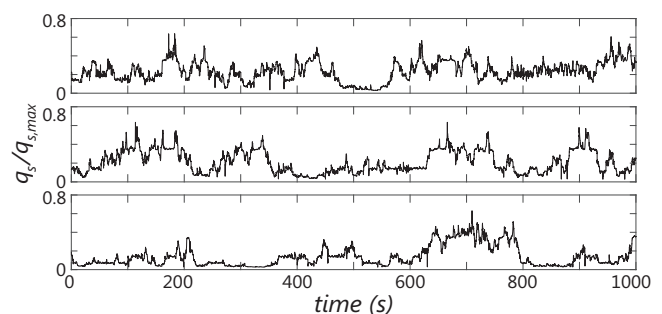
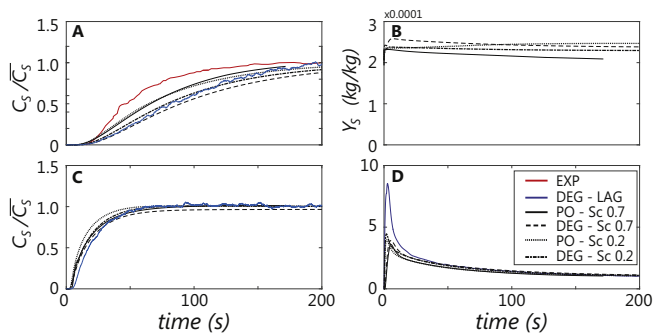


Fig. A2. Example of three randomly sampled particle tracks (unfiltered) in the CFD simulation, expressed in the specific substrate uptake rate  $q_s$  versus time.



**Fig. A3.** Mixing curves for all simulation setups. (A) Bottom probe. (B) Mean mass fraction of tracer. (C) Middle probe. (D) Top probe.

*The turbulent Schmidt number.* Whilst Coroneo et al. showed that the default  $Sc_T = 0.7$  suffices when assessing mixing in a single impeller stirred tank (Coroneo et al., 2011), several authors reported good agreement for  $\tau_{95}$  in multi-impeller vessels only when  $Sc_T$  was decreased to 0.1–0.2 (Montante et al., 2005; Gunyol et al., 2009; Delafosse et al., 2014; Haringa et al., 2016); significant over-predictions in  $\tau_{95}$  were observed when using  $Sc_T = 0.7$  (Bujalski et al., 2002; Jaworski et al., 2000; Jahoda et al., 2007; Kukuková et al., 2005). In line with Bujalski et al. (2002) and Jaworski et al. (2000), we believe the poor prediction of  $\tau_{95}$  in single-phase, multi-impeller simulations arises from an under-prediction of axial mass-exchange through the plane in between two impellers, where the flow is parallel and the mean axial velocity is negligible in case of single phase flow. The additional motion created by the gas seems to break this barrier for the current simulation, leading to a lesser influence of  $Sc_T$  on the overall mixing time, with no notable improvement in  $\tau_{95}$  by changing the value of  $Sc_T$ . The upward motion caused by gassing, as was illustrated by Vrabel et al. (1999), is indeed observed in the liquid velocity field (Fig. A4) in the current simulation. Overall, the dual circulation loops for each Rushton impeller are still clearly visible, indicating that despite the high gas fractions the flow induced by stirring dominates the flow by aeration.

The difference in  $\tau_{95}$  observed between the degassing and pressure outlet condition may furthermore be influenced by the placement of the feedpoint, close to the gas-holdup artifact arising from the boundary condition (observed in Fig. 2) (see Table A1).

## Appendix B. Regime sensitivity analysis

Because of the differences in mixing time between simulations with a pressure outlet boundary condition, and the simulations with a degassing boundary condition, the concentration gradient may differ somewhat between these cases. The turbulent Schmidt number will also influence the substrate gradient, by influencing the mixing time as well as local mixing behavior via the ‘amplification’ of turbulent diffusion. To study the influences of these simulation settings, the concentration gradient between four different cases has been compared.

Fig. B1 shows the global gradient in each case. Despite the significant differences in  $\tau_{95}$  between the four approaches, a similar gradient is observed in every case. The longer mixing time for the degassing simulation leads to an overall steeper gradient, resulting in a larger region where  $C_s < 5$  mg/L near the bottom, and a somewhat larger region where  $C_s > 80$  mg/L near the top, but the differences are comparatively small. This is reflected in the registered concentrations at the probe locations; the concentration at the top probe does differ significantly between the simulations due to the proximity of the feed point, where the exact gradient is very sensitive to details in the flow pattern. At the

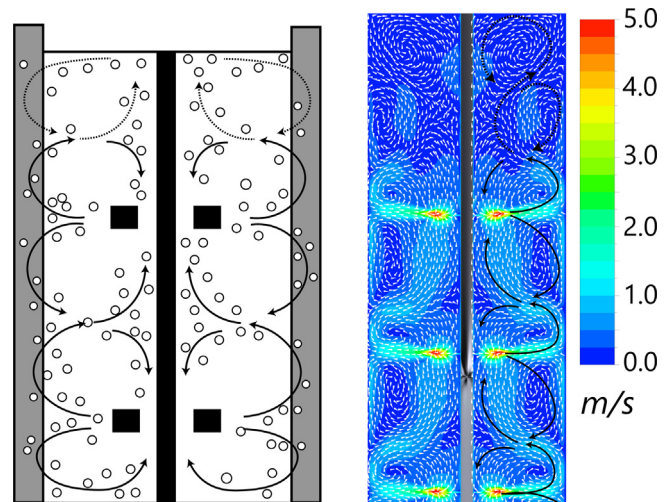


**Fig. A4.** Liquid flowfield calculated by CFD simulations (right) compared with the flowfield observed by Vrabel et al. (left; adapted from Vrabel et al., 2000).

middle and bottom probes, the differences between the simulation approaches are less pronounced.

The influence of the  $Sc_T$  is mainly visible in the downflowing jets originating from the impellers (most notably the 2nd). While the relatively high glucose stream carried in this jet is confined very near the wall for  $Sc_T = 0.7$ , it spreads significantly for  $Sc_T = 0.2$ . These observations are consistent between the pressure outlet and degassing situation.

Globally, the different simulation settings have little effect on the regime distribution (Fig. B2); only minor changes in the regime interface locations are observed in the vicinity at the impeller. The per regime residence time distributions are therefore not expected to differ significantly in terms of long term behavior, but they may show differences in short time behavior. These short, low amplitude variations likely have only a minor effect on the organism, but may significantly affect distribution statistics (like the mean RTD). It is therefore advised to remove such short term features, either during analysis using filtering procedures, or afterward by fitting only the long-time section of the RTDs in scale-down design.

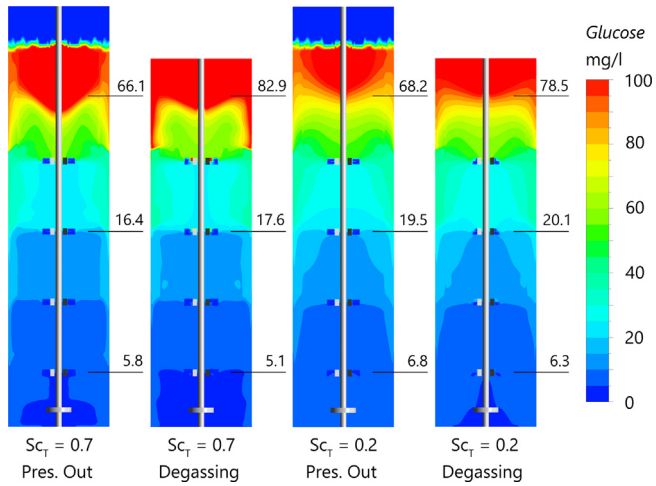
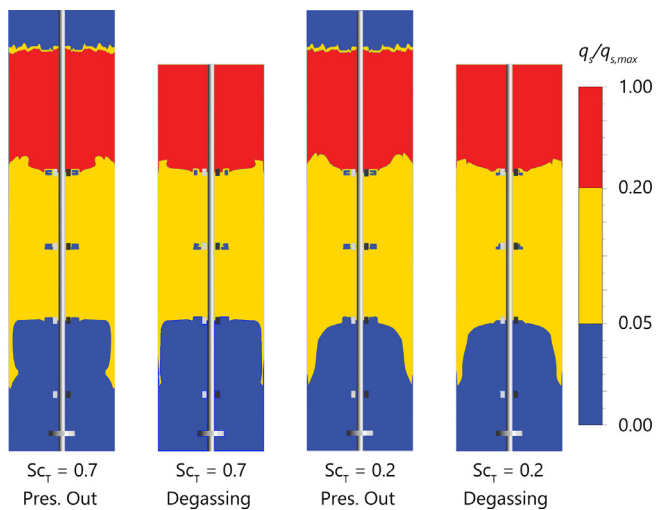
### B.1. Data filtering and smoothing

As prescribed by Haringa et al. (2016), the organism lifelines were smoothed using a moving-average filter, with a filter window based on the Lagrangian timescale  $\bar{\tau}_l = 0.15\bar{k}/\bar{\epsilon} = 0.18$  s. Here,  $\bar{k}$  and  $\bar{\epsilon}$  are the volume-averaged turbulent kinetic energy and volume-averaged energy dissipation rate. This filter smooths out turbulent variations in  $C_s$  which are responsible for low-amplitude noise; this turbulent noise is expected to have little influence on the state of the organism, which is a notion supported by DNS simulations of organisms in homogeneous turbulence (Linkes et al., 2014). The noise removal reduces the skewing of the RTDs towards short-timescale events: in the unfiltered data many consecutive crossings of the regime interface are registered due to the turbulent noise. Again, these rapid, low amplitude  $C_s$  variations are expected to have no significant effect on the organism. Applying the smoothing filter similarly removes noisy outliers during the registration of  $\Omega_{s,res}$ .

While being reduced in number, the smoothed data may still contain rapid consecutive low-amplitude crossings of a regime interface when sharp regime interfaces are used. To remove these events, a dispersed-boundary filter (essentially an overlap region between the regimes rather than a sharp interface) was used to filter out a significant portion of low amplitude rapid oscillations. In

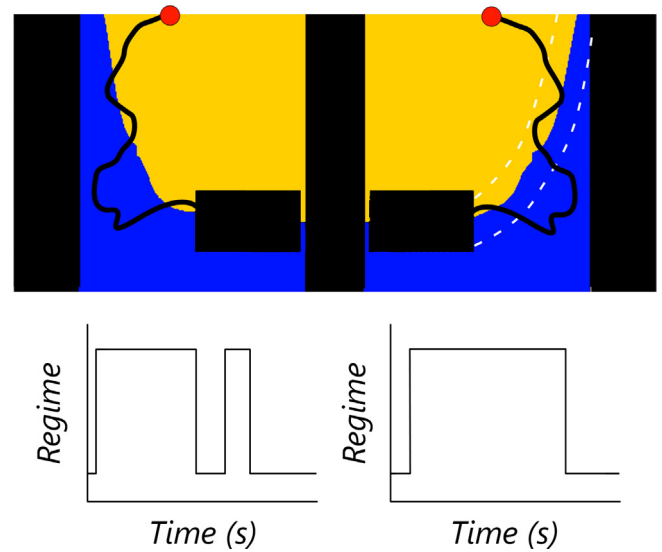
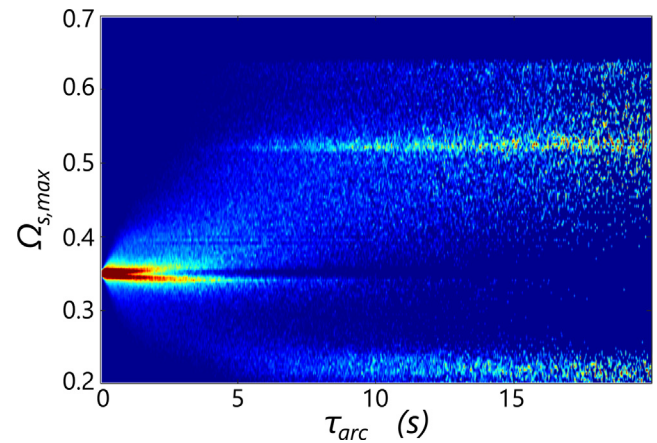
**Table A1**95% mixing time for each probe location for all Eulerian simulations, and the Lagrangian mixing simulation (executed with degassing,  $Sc_T = 0.7$ ).

| Case       | PO, $Sc = 0.7$ | DEG, $Sc = 0.7$ | PO, $Sc = 0.2$ | DEG, $Sc = 0.2$ | DEG, Lagrange |
|------------|----------------|-----------------|----------------|-----------------|---------------|
| Top (s)    | 156.6          | 193.8           | 194.3          | > 200           | 182.4         |
| Middle (s) | 56.6           | 77.9            | 39.7           | 48.8            | 53.5          |
| Bottom (s) | 168.7          | 235.4           | 203.3          | > 200           | 182.8         |

**Fig. B1.** Comparison of concentration gradients for different outlet boundary conditions and values of the turbulent Schmidt number  $Sc_T$ . Concentrations at the probe location are presented right of every contour map.**Fig. B2.** Comparison of the regime distribution for the different simulation setups.

this case, a 1% filter was used at the regime 1 - regime 2 interface and a 0.5% filter at the regime 2 - regime 3 interface; using a 1% filter here would lead to an excessively large overlap zone. This 0.5% filter in essence means that a particle must cross the boundary  $q_s/q_{s,max} = 0.055$  when moving from regime 3 to 2, and  $q_s/q_{s,max} = 0.045$  when moving in the converse direction. This is graphically outlined in Fig. B3. For further details on the disperse-boundary filter, please refer to the supplementary data of Haringa et al. (2016).

As a final filtering step, a rate-of-change filter was implemented; particles touching upon the trailing vortices erroneously register starvation conditions at every impeller due to the absence of substrate in the vortex, leading to nonphysical concentration jumps. Occasions where  $q_s/q_{s,max}$  changed from  $> 0.1$  to  $< 0.05$

**Fig. B3.** Graphical layout of the dispersed boundary filter. On the left, the original trajectory moving is shown oscillating between regimes 2 and 3. Right, the same trajectory is showing with the dispersed boundary filter (dashed lines) imposed; the low-amplitude oscillation in  $q_s/q_{s,max}$  is removed by the filter, with the particle being registered in the blue regime (regime 3) until the inner dashed line is crossed (reproduced with permission from Haringa et al., 2016).**Fig. B4.** Arc-magnitude  $\Omega_{s,max}$  versus arc-time  $\tau_{arc}$  for regime 1, showing banded behavior similar to the analysis of regime 2, but with significantly more scatter due to the stronger gradient existing near the feedpoint.

within a time-step were removed by upwind interpolation, replacing the erroneous value with the value registered in the previous timestep.

### B.2. Arc-analysis for regime 1

As noted in the main text, an arc analysis was conducted for the ethanol-producing regime (regime 1) since  $q_s$  is sensitive to variations in  $C_s$  in this region. The arc-time distribution ( $\tau_{arc}$ ) was reported in the main text, here, the  $\Omega_{s,max}$  versus  $\tau_{arc}$  plot is shown in Fig. B4. This distribution lies in between the distributions

registered for regime 2 and *P. chrysogenum*, regime 2 reported in Fig. 6 of the main text. Similar to regime 2 of the current case, 2 clear bands are visible in the distribution. Still, there is significant scatter, similar to the *P. chrysogenum* case. This indicates that the circulation loops in regime 1 are less homogeneous than in the regime 2 region, which can be understood considering the proximity to the feed-point, where strong gradients exist due to dilution effects (main text, Fig. 2). Still, the overall banded behavior does show how organisms move between loops; they tend to stick within the loop directly around the reference value for  $t < 5$  s, with essentially all particles on a trajectory lasting  $> 5$  s jump to a loop close to the regime 2 boundary (downward) or feed point (upward). In Fig. 7 of the main paper, these two modes are also clearly visible in the  $\tau_{arc}$  distribution, with an overlap region between 3 and 5 s.

## References

- Abel, C., Hübner, U., Schügerl, K., 1994. Transient behaviour of Baker's yeast during enforced periodical variation of dissolved oxygen concentration. *J. Biotechnol.* 32 (1), 45–57. [http://dx.doi.org/10.1016/0168-1656\(94\)90119-8](http://dx.doi.org/10.1016/0168-1656(94)90119-8). ISSN 01681656 <<http://linkinghub.elsevier.com/retrieve/pii/0168165694901198>>.
- Barigou, M., Greaves, M., 1992. Bubble-size distributions in a mechanically agitated gasliquid contactor. *Chem. Eng. Sci.* 47 (8), 2009–2025. [http://dx.doi.org/10.1016/0009-2509\(92\)80318-7](http://dx.doi.org/10.1016/0009-2509(92)80318-7). ISSN 00092509 <<http://www.sciencedirect.com/science/article/pii/0009250992803187>> <<http://linkinghub.elsevier.com/retrieve/pii/0009250992803187>>.
- Bujalski, W., Jaworski, Z., Nienow, A., 2002. CFD study of homogenization with dual Rushton turbines—comparison with experimental results. *Chem. Eng. Res. Des.* 80 (1), 97–104. <http://dx.doi.org/10.1205/026387602753393402>. ISSN 02638762 <<http://www.sciencedirect.com/science/article/pii/S0263876202721540>>.
- Choi, B.S., Wan, B., Philyaw, S., Dhanasekharan, K., Ring, T.A., 2004. Residence time distributions in a stirred tank: comparison of CFD predictions with experiment. *Ind. Eng. Chem. Res.* 43 (20), 6548–6556. <http://dx.doi.org/10.1021/ie0308240>. ISSN 0888-5885.
- Coroneo, M., Montante, G., Paglianti, A., Magelli, F., 2011. CFD prediction of fluid flow and mixing in stirred tanks: numerical issues about the RANS simulations. *Comput. Chem. Eng.* 35 (10), 1959–1968. <http://dx.doi.org/10.1016/j.compchemeng.2010.12.007>. ISSN 00981354 <<http://www.sciencedirect.com/science/article/pii/S0098135410003686>>.
- de Jonge, L.P., Buijs, N.A.A., ten Pierick, A., Deshmukh, A., Zhao, Z., Kiel, J.A.K.W., Heijnen, J.J., van Gulik, W.M., 2011. Scale-down of penicillin production in *Penicillium chrysogenum*. *Biotechnol. J.* 6 (8), 944–958. <http://dx.doi.org/10.1002/biot.201000409>. ISSN 1860-7314 <<http://www.ncbi.nlm.nih.gov/pubmed/21751388>>.
- Delafosse, A., Collignon, M.-L., Calvo, S., Delvigne, F., Crine, M., Thonart, P., Toye, D., 2014. CFD-based compartment model for description of mixing in bioreactors. *Chem. Eng. Sci.* 106, 76–85 <<http://www.sciencedirect.com/science/article/pii/S0009250913007690>>.
- Delafosse, A., Calvo, S., Collignon, M.-L., Delvigne, F., Crine, M., Toye, D., 2015. Euler-Lagrange approach to model heterogeneities in stirred tank bioreactors—comparison to experimental flow characterization and particle tracking. *Chem. Eng. Sci.* 134, 457–466. <http://dx.doi.org/10.1016/j.ces.2015.05.045>. ISSN 00092509 <<http://www.sciencedirect.com/science/article/pii/S0009250915003851>>.
- Delvigne, F., Destain, J., Thonart, P., 2006. A methodology for the design of scale-down bioreactors by the use of mixing and circulation stochastic models. *Biochem. Eng. J.* 28 (3), 256–268. <http://dx.doi.org/10.1016/j.bej.2005.11.009>. ISSN 1369703X <<http://www.sciencedirect.com/science/article/pii/S1369703X0500358X>>.
- Enfors, S.-O., Jahic, M., Rozkov, A., Xu, B., Hecker, M., Jürgen, B., Krüger, E., Schweder, T., Hamer, G., O'Beirne, D., Noisommit-Rizzi, N., Reuss, M., Boone, L., Hewitt, C., McFarlane, C., Nienow, A., Kovacs, T., Trägårdh, C., Fuchs, L., Revstedt, J., Friberg, P., Hjertager, B., Blomsten, G., Skogman, H., Hjort, S., Hoeks, F., Lin, H.-Y., Neubauer, P., van der Lans, R., Luyben, K., Vrabel, P., Manelius, Å., 2001. Physiological responses to mixing in large scale bioreactors. *J. Biotechnol.* 85 (2), 175–185. [http://dx.doi.org/10.1016/S0168-1656\(00\)00365-5](http://dx.doi.org/10.1016/S0168-1656(00)00365-5). ISSN 01681656 <<http://www.sciencedirect.com/science/article/pii/S0168165600003655>> <<http://linkinghub.elsevier.com/retrieve/pii/S0168165600003655>>.
- George, S., Larsson, G., Enfors, S.O., 1993. A scale-down two-compartment reactor with controlled substrate oscillations: metabolic response of *Saccharomyces cerevisiae*. *Bioprocess Eng.* 9 (6), 249–257. <http://dx.doi.org/10.1007/BF01061530>. ISSN 0178-515X <<http://link.springer.com/10.1007/BF01061530>>.
- George, S., Larsson, G., Olsson, K., Enfors, S.-O., 1998. Comparison of the Baker's yeast process performance in laboratory and production scale. *Bioprocess Eng.* 18 (2), 135–142. <http://dx.doi.org/10.1007/PL00008979>. ISSN 0178-515X <<http://link.springer.com/10.1007/PL00008979>>.
- Gimbu, J., Rielly, C., Nagy, Z., 2009. Modelling of mass transfer in gasliquid stirred tanks agitated by Rushton turbine and CD-6 impeller: a scale-up study. *Chem. Eng. Res. Des.* 87 (4), 437–451. <http://dx.doi.org/10.1016/j.cherd.2008.12.017>. ISSN 02638762.
- Gunyol, O., Mudde, R.F., 2009. Computational study of hydrodynamics of a standard stirred tank reactor and a large-scale multi-impeller fermenter. *Int. J. Multiscale Comput. Eng.* 7 (6), 559–576. ISSN 1543-1649.
- Gunyol, O., Noorman, H.J., Mudde, R.F., 2009. CFD simulations of a large-scale fermenter with multiple impellers. In: Chauki, P., Tanguy, J. (Ed.), Proceedings of the 9th International Conference on Gas-Liquid Solid Reactor Engineering, Montreal, pp. 1–4.
- Haringa, C., Tang, W., Deshmukh, A.T., Xia, J., Reuss, M., Heijnen, J.J., Mudde, R.F., Noorman, H.J., 2016. Euler-Lagrange computational fluid dynamics for (bio) reactor scale-down: an analysis of organism life-lines. *Eng. Life Sci.* <http://dx.doi.org/10.1002/elsc.201600061>. ISSN 16180240.
- Haringa, C., Noorman, H.J., Mudde, R.F., 2017. Lagrangian modeling of hydrodynamic kinetic interactions in (bio)chemical reactors: practical implementation and setup guidelines. *Chem. Eng. Sci.* 157, 159–168. <http://dx.doi.org/10.1016/j.ces.2016.07.031>. ISSN 00092509.
- Heijnen, J., Romein, B., 1995. Derivation of kinetic equations for growth on single substrates based on general properties of a simple metabolic network. *Biotechnol. Prog.* 11 (6), 712–716. <http://dx.doi.org/10.1021/bp00036a018>.
- Heins, A.-L., Lencastre Fernandes, R., Gernaey, K.V., Lantz, A.E., 2015. Experimental and in silico investigation of population heterogeneity in continuous *Saccharomyces cerevisiae* scale-down fermentation in a two-compartment setup. *J. Chem. Technol. Biotechnol.* 90 (2), 324–340. <http://dx.doi.org/10.1002/jctb.4532>. ISSN 02682575 <<http://doi.wiley.com/10.1002/jctb.4532>>.
- Ishii, M., Zuber, N., 1979. Drag coefficient and relative velocity in bubbly, droplet or particulate flows. *AIChE J.* 25 (5), 843–855. <http://dx.doi.org/10.1002/aic.690250513>. ISSN 0001-1541 <<http://doi.wiley.com/10.1002/aic.690250513>>.
- Jahoda, M., Moštk, M., Kukuková, A., Macho, V., 2007. CFD modelling of liquid homogenization in stirred tanks with one and two impellers using large eddy simulation. *Chem. Eng. Res. Des.* 85 (5), 616–625. <http://dx.doi.org/10.1205/cherd06183>. ISSN 02638762 <<http://www.sciencedirect.com/science/article/pii/S0263876207730915>>.
- Jaworski, Z., Bujalski, W., Otomo, N., Nienow, A., 2000. CFD study of homogenization with dual Rushton turbines—comparison with experimental results. *Chem. Eng. Res. Des.* 78 (3), 327–333. <http://dx.doi.org/10.1205/026387600527437>. ISSN 02638762 <<http://www.sciencedirect.com/science/article/pii/S026387620071896X>>.
- Kukuková, A., Moštk, M., Jahoda, M., Macho, V., 2005. CFD prediction of flow and homogenization in a stirred vessel: Part I vessel with one and two impellers. *Chem. Eng. Technol.* 28 (10), 1125–1133. <http://dx.doi.org/10.1002/ceat.200500094>. ISSN 0930-7516 <<http://doi.wiley.com/10.1002/ceat.200500094>>.
- Laakkonen, M., Moilanen, P., Miettinen, T., Saari, K., Honkanen, M., Saarenrinne, P., Aittamaa, J., 2005a. Local bubble size distributions in agitated vessel. *Chem. Eng. Res. Des.* 83 (1), 50–58. <http://dx.doi.org/10.1205/cherd.04122>. ISSN 02638762 <<http://www.sciencedirect.com/science/article/pii/S026387620572671X>> <<http://linkinghub.elsevier.com/retrieve/pii/S026387620572671X>>.
- Laakkonen, M., Honkanen, M., Saarenrinne, P., Aittamaa, J., 2005b. Local bubble size distributions, gasliquid interfacial areas and gas holdups in a stirred vessel with particle image velocimetry. *Chem. Eng. J.* 109 (1–3), 37–47. <http://dx.doi.org/10.1016/j.cej.2005.03.002>. ISSN 13858947 <<http://www.sciencedirect.com/science/article/pii/S1385894705000811>> <<http://linkinghub.elsevier.com/retrieve/pii/S1385894705000811>>.
- Lamont, J.C., Scott, D.S., 1970. An eddy cell model of mass transfer into the surface of a turbulent liquid. *AIChE J.* 16 (4), 513–519. <http://dx.doi.org/10.1002/aic.690160403>. ISSN 0001-1541 <<http://doi.wiley.com/10.1002/aic.690160403>>.
- Lapin, A., Müller, D., Reuss, M., 2004. Dynamic behavior of microbial populations in stirred bioreactors simulated with Euler-Lagrange methods: traveling along the lifelines of single cells. *Ind. Eng. Chem. Res.* 43 (16), 4647–4656. <http://dx.doi.org/10.1021/ie030786k>. ISSN 0888-5885 <<http://pubs.acs.org/doi/abs/10.1021/ie030786k>>.
- Lapin, A., Schmid, J., Reuss, M., 2006. Modeling the dynamics of *E. coli* populations in the three-dimensional turbulent field of a stirred-tank bioreactor—a structured-segregated approach. *Chem. Eng. Sci.* 61 (14), 4783–4797. <http://dx.doi.org/10.1016/j.ces.2006.03.003>. ISSN 00092509 <<http://www.sciencedirect.com/science/article/pii/S0009250906001606>> <<http://linkinghub.elsevier.com/retrieve/pii/S0009250906001606>>.
- Larsson, G., Trnkvišt, M., Wernersson, E.S., Trgrdh, C., Noorman, H., Enfors, S.O., 1996. Substrate gradients in bioreactors: origin and consequences. *Bioprocess Eng.* 14 (6), 281–289. <http://dx.doi.org/10.1007/BF00369471>. ISSN 0178-515X <<http://link.springer.com/10.1007/BF00369471>>.
- Lee, B.W., Dudukovic, M.P., 2014. Determination of flow regime and gas holdup in gasliquid stirred tanks. *Chem. Eng. Sci.* 109, 264–275. <http://dx.doi.org/10.1016/j.ces.2014.01.032>. ISSN 00092509.
- Lemoine, A., Maya Martinez-Itrralde, N., Spann, R., Neubauer, P., Junne, S., 2015. Response of *Corynebacterium glutamicum* exposed to oscillating cultivation conditions in a two- and a novel three-compartment scale-down bioreactor. *Biotechnol. Bioeng.* 112 (6), 1220–1231. <http://dx.doi.org/10.1002/bit.25543>. ISSN 1097-0290 <<http://www.ncbi.nlm.nih.gov/pubmed/25728062>>.
- Limberg, M.H., Pooth, V., Wiechert, W., Oldiges, M., 2016. Plug flow vs. stirred tank reactor flow characteristics in two compartment scale down bioreactor: Setup specific influence on the metabolic phenotype and bioprocess performance of *Corynebacterium glutamicum*. *Eng. Life Sci.* <http://dx.doi.org/10.1002/elsc.201500142>. ISSN 16180240 <<http://doi.wiley.com/10.1002/elsc.201500142>>.

- Linkèš, M., Fede, P., Morchain, J., Schmitz, P., 2014. Numerical investigation of subgrid mixing effects on the calculation of biological reaction rates. *Chem. Eng. Sci.* 116, 473–485. <http://dx.doi.org/10.1016/j.ces.2014.05.005>. ISSN 00092509 <<http://www.sciencedirect.com/science/article/pii/S0009250914002152>>.
- Lübbert, A., Larson, B., 1990. Detailed investigations of the multiphase flow in airlift tower loop reactors. *Chem. Eng. Sci.* 45 (10), 3047–3053. [http://dx.doi.org/10.1016/0009-2509\(90\)80051-F](http://dx.doi.org/10.1016/0009-2509(90)80051-F). ISSN 00092509 <<http://www.sciencedirect.com/science/article/pii/S000925099080051-F>>.
- Luo, H., Svendsen, H.F., 1996. Theoretical model for drop and bubble breakup in turbulent dispersions. *AIChE J.* 42 (5), 1225–1233. <http://dx.doi.org/10.1002/aic.690420505>. ISSN 0001-1541 <<http://doi.wiley.com/10.1002/aic.690420505>>.
- McClure, D.D., Kavanagh, J.M., Fletcher, D.F., Barton, G.W., 2016. Characterizing bubble column bioreactor performance using computational fluid dynamics. *Chem. Eng. Sci.* 144, 58–74. <http://dx.doi.org/10.1016/j.ces.2016.01.016>. ISSN 00092509 <<http://linkinghub.elsevier.com/retrieve/pii/S0009250916000257>>.
- Montante, G., Moštek, M., Jahoda, M., Magelli, F., 2005. CFD simulations and experimental validation of homogenisation curves and mixing time in stirred Newtonian and pseudoplastic liquids. *Chem. Eng. Sci.* 60 (8–9), 2427–2437. <http://dx.doi.org/10.1016/j.ces.2004.11.020>. ISSN 00092509 <<http://www.sciencedirect.com/science/article/pii/S0009250904009169>>.
- Neubauer, P., Junne, S., 2010. Scale-down simulators for metabolic analysis of large-scale bioprocesses. *Curr. Opin. Biotechnol.* 21 (1), 114–121. <http://dx.doi.org/10.1016/j.copbio.2010.02.001>. ISSN 1879-0429 <<http://www.sciencedirect.com/science/article/pii/S0958166910000157>> <<http://www.ncbi.nlm.nih.gov/pubmed/20185293>>.
- Noorman, H., 2011. An industrial perspective on bioreactor scale-down: what we can learn from combined large-scale bioprocess and model fluid studies. *Biotechnol. J.* 6 (8), 934–943. <http://dx.doi.org/10.1002/biot.201000406>. ISSN 1860-7314 <<http://www.ncbi.nlm.nih.gov/pubmed/21695785>>.
- Oosterhuis, N.M., Kossen, N.W., 1984. Dissolved oxygen concentration profiles in a production-scale bioreactor. *Biotechnol. Bioeng.* 26 (5), 546–550. <http://dx.doi.org/10.1002/bit.260260522>. ISSN 0006-3592 <<http://www.ncbi.nlm.nih.gov/pubmed/18553353>>.
- Pham, H.T.B., Larsson, G., Enfors, S.-O., 1998. Growth and energy metabolism in aerobic fed-batch cultures of *Saccharomyces cerevisiae*: Simulation and model verification. *Biotechnol. Bioeng.* 60 (4), 474–482. [http://dx.doi.org/10.1002/\(SICI\)1097-0290\(19981120\)60:4<474::AID-BIT9>3.0.CO;2-J](http://dx.doi.org/10.1002/(SICI)1097-0290(19981120)60:4<474::AID-BIT9>3.0.CO;2-J). ISSN 00063592 <<http://doi.wiley.com/10.1002/%28SICI%291097-0290%2819981120%2960%3A4%3C474%3A%3AAID-BIT9%3E3.0.CO%3B2-J>>.
- Pigou, M., Morchain, J., 2015. Investigating the interactions between physical and biological heterogeneities in bioreactors using compartment, population balance and metabolic models. *Chem. Eng. Sci.* 126, 267–282.
- Postma, E., Verduyn, C., Scheffers, W.A., Van Dijken, J.P., 1989a. Enzymic analysis of the crabtree effect in glucose-limited chemostat cultures of *Saccharomyces cerevisiae*. *Appl. Environ. Microbiol.* 55 (2), 468–477. ISSN 0099-2240 <<http://www.ncbi.nlm.nih.gov/pubmed/2566299>> <<http://www.pubmedcentral.nih.gov/articlerender.fcgi?artid=PMC184133>>.
- Postma, E., Alexander Scheffers, W., Van Dijken, J.P., 1989b. Kinetics of growth and glucose transport in glucose-limited chemostat cultures of *Saccharomyces cerevisiae* CBS 8066. *Yeast* 5 (3), 159–165. <http://dx.doi.org/10.1002/yea.320050305>. ISSN 0749-503X <<http://doi.wiley.com/10.1002/yea.320050305>>.
- Suarez-Mendez, C.A., 2013. Dynamics of Storage Carbohydrates Metabolism in *S. cerevisiae*: A Quantitative Analysis (Ph.D. Thesis). Delft University of Technology.
- Suarez-Mendez, C., Sousa, A., Heijnen, J., Wahl, A., 2014. Fast feast/famine cycles for studying microbial physiology under dynamic conditions: a case study with *Saccharomyces cerevisiae*. *Metabolites* 4 (2), 347–372. <http://dx.doi.org/10.3390/metabo4020347>. ISSN 2218-1989 <<http://www.mdpi.com/2218-1989/4/2/347>>.
- Sweere, A.P.J., Mesters, J.R., Janse, L., Luyben, K.C.A.M., Kossen, N.W.F., 1988a. Experimental simulation of oxygen profiles and their influence on baker's yeast production: I. One-fermentor system. *Biotechnol. Bioeng.* 31 (6), 567–578. <http://dx.doi.org/10.1002/bit.260310609>. ISSN 0006-3592 <<http://doi.wiley.com/10.1002/bit.260310609>>.
- Sweere, A.P.J., Janse, L., Luyben, K.C.A.M., Kossen, N.W.F., 1988b. Experimental simulation of oxygen profiles and their influence on baker's yeast production: II. Two-fermentor system. *Biotechnol. Bioeng.* 31 (6), 579–586. <http://dx.doi.org/10.1002/bit.260310610>. ISSN 0006-3592 <<http://doi.wiley.com/10.1002/bit.260310610>>.
- Sweere, A.P.J., Mesters, J.R., Janse, L., Luyben, K.C.A.M., Kossen, N.W.F., 1988c. Experimental simulation of oxygen profiles and their influence on baker's yeast production: I. One-fermentor system. *Biotechnol. Bioeng.* 31 (6), 567–578. <http://dx.doi.org/10.1002/bit.260310609>. ISSN 0006-3592 <<http://doi.wiley.com/10.1002/bit.260310609>>.
- Sweere, A.P.J., Matla, Y.A., Zandvliet, J., Luyben, K.C.A.M., Kossen, N.W.F., 1988d. Experimental simulation of glucose fluctuations. *Appl. Microbiol. Biotechnol.* 28 (2), 109–115. <http://dx.doi.org/10.1007/BF00694297>. ISSN 0175-7598 <<http://link.springer.com/10.1007/BF00694297>>.
- van der Lans, R.G., van't Riet, K., 2011. Mixing in bioreactor vessels. In: Moo-Young, M. (Ed.), *Comprehensive Biotechnology. Engineering Fundamentals of Biotechnology*, vol. 2, second ed., Elsevier, Amsterdam, pp. 63–80 (chap. 2.07). <http://dx.doi.org/10.1016/B978-0-08-088504-9.00083->.
- van Kleeff, B., Kuennen, J., Heijnen, J., 1996. Heat flux measurements for the fast monitoring of dynamic responses to glucose additions by yeasts that were subjected to different feeding regimes in continuous culture. *Biotechnol. Prog.* 12 (4), 510–518. <http://dx.doi.org/10.1021/bp960033b>. ISSN 8756-7938 <<http://doi.wiley.com/10.1021/bp960033b>>.
- Van Urk, H., Postma, E., Scheffers, W.A., Van Dijken, J.P., 1989. Glucose transport in crabtree-positive and crabtree-negative yeasts. *Microbiology* 135 (9), 2399–2406. <http://dx.doi.org/10.1099/00221287-135-9-2399>. ISSN 1350-0872 <<http://mic.microbiologyresearch.org/content/journal/micro/10.1099/00221287-135-9-2399>>.
- Verduyn, C., Postma, E., Scheffers, W.A., van Dijken, J.P., 1990. Physiology of *Saccharomyces cerevisiae* in anaerobic glucose-limited chemostat cultures. *J. Gener. Microbiol.* 136 (3), 395–403. <http://dx.doi.org/10.1099/00221287-136-3-395>. ISSN 0022-1287 <<http://mic.microbiologyresearch.org/content/journal/micro/10.1099/00221287-136-3-395>>.
- Verduyn, C., Postma, E., Scheffers, W.A., Van Dijken, J.P., 1992. Effect of benzoic acid on metabolic fluxes in yeasts: a continuous-culture study on the regulation of respiration and alcoholic fermentation. *Yeast* 8 (7), 501–517. <http://dx.doi.org/10.1002/yea.320080703>. ISSN 0749-503X <<http://doi.wiley.com/10.1002/yea.320080703>>.
- Vrábel, P., Van der Lans, R., Cui, Y., Luyben, K., 1999. Compartment model approach: Mixing in large scale aerated reactors with multiple impellers. *Chem. Eng. Res. Des.* 77 (4), 291–302. <http://dx.doi.org/10.1205/026387699526223>. ISSN 02638762 <<http://www.sciencedirect.com/science/article/pii/S0263876299717892>>.
- Vrábel, P., van der Lans, R.G., Luyben, K.C., Boon, L., Nienow, A.W., 2000. Mixing in large-scale vessels stirred with multiple radial or radial and axial up-pumping impellers: modelling and measurements. *Chem. Eng. Sci.* 55 (23), 5881–5896. [http://dx.doi.org/10.1016/S0009-2509\(00\)00175-5](http://dx.doi.org/10.1016/S0009-2509(00)00175-5). ISSN 00092509 <<http://www.sciencedirect.com/science/article/pii/S0009250900001755>>.
- Vrábel, P., van der Lans, R.G., van der Schot, F.N., Luyben, K.C., Xu, B., Enfors, S.-O., 2001. CMA: integration of fluid dynamics and microbial kinetics in modelling of large-scale fermentations. *Chem. Eng. J.* 84 (3), 463–474. [http://dx.doi.org/10.1016/S1385-8947\(00\)00271-0](http://dx.doi.org/10.1016/S1385-8947(00)00271-0). ISSN 13858947 <<http://www.sciencedirect.com/science/article/pii/S1385894700002710>>.
- Wang, T., Wang, J., Jin, Y., 2005. Population balance model for gasliquid flows: influence of bubble coalescence and breakup models. *Ind. Eng. Chem. Res.* 44 (19), 7540–7549. <http://dx.doi.org/10.1021/ie0489002>. ISSN 0888-5885 <<http://pubs.acs.org/doi/abs/10.1021/ie0489002>>.
- Wang, G., Tang, W., Xia, J., Chu, J., Noorman, H., van Gulik, W.M., 2015. Integration of microbial kinetics and fluid dynamics toward model-driven scale-up of industrial bioprocesses. *Eng. Life Sci.* 15 (1), 20–29. <http://dx.doi.org/10.1002/elsc.201400172>. ISSN 16180240 <<http://doi.wiley.com/10.1002/elsc.201400172>>.
- Ying Lin, H., Neubauer, P., 2000. Influence of controlled glucose oscillations on a fed-batch process of recombinant *Escherichia coli*. *J. Biotechnol.* 79 (1), 27–37. [http://dx.doi.org/10.1016/S0168-1656\(00\)00217-0](http://dx.doi.org/10.1016/S0168-1656(00)00217-0). ISSN 01681656.